Article

Tertiary lymphoid structures improve immunotherapy and survival in melanoma

https://doi.org/10.1038/s41586-019-1914-8

Received: 5 February 2019

Accepted: 4 December 2019

Published online: 15 January 2020

There are amendments to this paper

Rita Cabrita[1,12], Martin Lauss[1,12], Adriana Sanna[1], Marco Donia[2], Mathilde Skaarup Larsen[3], Shamik Mitra[1], Iva Johansson[1], Bengt Phung[1], Katja Harbst[1], Johan Vallon-Christersson[1], Alison van Schoiack[4], Kristina Lövgren[1], Sarah Warren[4], Karin Jirström[1], Håkan Olsson[1], Kristian Pietras[5], Christian Ingvar[6], Karolin Isaksson[6], Dirk Schadendorf[7], Henrik Schmidt[8], Lars Bastholt[9], Ana Carneiro[1,10], Jennifer A. Wargo[11], Inge Marie Svane[2] & Göran Jönsson[1]*

Checkpoint blockade therapies that reactivate tumour-associated T cells can induce durable tumour control and result in the long-term survival of patients with advanced cancers[1]. Current predictive biomarkers for therapy response include high levels of intratumour immunological activity, a high tumour mutational burden and specific characteristics of the gut microbiota[2,3]. Although the role of T cells in antitumour responses has thoroughly been studied, other immune cells remain insufficiently explored. Here we use clinical samples of metastatic melanomas to investigate the role of B cells in antitumour responses, and find that the co-occurrence of tumour-associated $CD8^+$ T cells and $CD20^+$ B cells is associated with improved survival, independently of other clinical variables. Immunofluorescence staining of CXCR5 and CXCL13 in combination with CD20 reveals the formation of tertiary lymphoid structures in these $CD8^+CD20^+$ tumours. We derived a gene signature associated with tertiary lymphoid structures, which predicted clinical outcomes in cohorts of patients treated with immune checkpoint blockade. Furthermore, B-cell-rich tumours were accompanied by increased levels of $TCF7^+$ naive and/or memory T cells. This was corroborated by digital spatial-profiling data, in which T cells in tumours without tertiary lymphoid structures had a dysfunctional molecular phenotype. Our results indicate that tertiary lymphoid structures have a key role in the immune microenvironment in melanoma, by conferring distinct T cell phenotypes. Therapeutic strategies to induce the formation of tertiary lymphoid structures should be explored to improve responses to cancer immunotherapy.

In addition to T cells, the main component of the adaptive immune system consists of B cells. B cells localized in so-called tertiary lymphoid structures (TLSs)—which have been identified in several types of cancer, including melanoma[4–6]—may improve antigen presentation, increase cytokine-mediated signalling, release tumour-specific antibodies, are associated with improved prognosis[7] and, to some extent, with clinical responses to CTLA4[5]. Additional evidence on the importance of TLSs in the tumour immune microenvironment is provided in the accompanying Articles[8,9]. In our analysis of the immune microenvironment of melanoma tumours, we found infiltration of $CD8^+$ T cells in 33% of cases: 25% of the tumours had $CD8^+$ T cells localized in clusters, and 42% were devoid of $CD8^+$ T cells (Extended Data Table 1). By contrast, we found $CD20^+$ B cell clusters in 25% of the cases and such clusters consisted of both $Ki67^+$ and $Ki67^-$ B cells (Fig. 1a), which suggests that some B cells are activated and proliferating[10]. Notably, $CD20^+$ B cell clusters were in all cases surrounded mainly by $CD4^+$T cells, which indicates formation of TLSs (Extended Data Fig. 1a). We then analysed whether these $CD20^+$ B cell clusters have similarities to bona fide TLSs. Known molecular markers of TLS formation include increased expression of CXCL13, CXCR5 and DC-LAMP[11]. These markers were all upregulated in transcriptomic data from matched tumour tissue (Fig. 1b). Moreover, immunofluorescence staining of two known TLS markers (CXCR5 and CXCL13), in combination with CD20, supported the notion that these $CD20^+$ B cell clusters have molecular properties that have been described as necessary for TLS formation[11] (Fig. 1c). By contrast, $CD8^+$ T cells were localized mainly outside of such TLSs, but the presence of TLSs was in all cases coupled with tumour-associated $CD8^+$ T cells (Fig. 1a, Extended Data Table 1). The formation of TLSs may indicate that tumour antigens are recognized by the immune system. The inability of the immune system to completely eradicate the tumour would

[1]Department of Clinical Sciences, Division of Oncology and Pathology, Lund University Cancer Center, Lund University, Lund, Sweden. [2]National Center for Cancer Immune Therapy, Department of Oncology, Copenhagen University Hospital, Herlev, Denmark. [3]Department of Clinical Pathology, Herlev University Hospital, Herlev, Denmark. [4]NanoString Technologies, Seattle, WA, USA. [5]Division of Translational Cancer Research, Department of Laboratory Medicine, Lund University Cancer Center, Lund University, Lund, Sweden. [6]Department of Surgery, Skåne University Hospital, Lund, Sweden. [7]Department of Dermatology, University Hospital of Essen, Essen, Germany. [8]Department of Oncology, Århus University Hospital, Aarhus, Denmark. [9]Department of Oncology, Odense University Hospital, Odense, Denmark. [10]Department of Oncology, Skåne University Hospital, Lund, Sweden. [11]Department of Surgical Oncology, MD Anderson Cancer Center, Houston, TX, USA. [12]These authors contributed equally: Rita Cabrita, Martin Lauss. *e-mail: goran_b.jonsson@med.lu.se

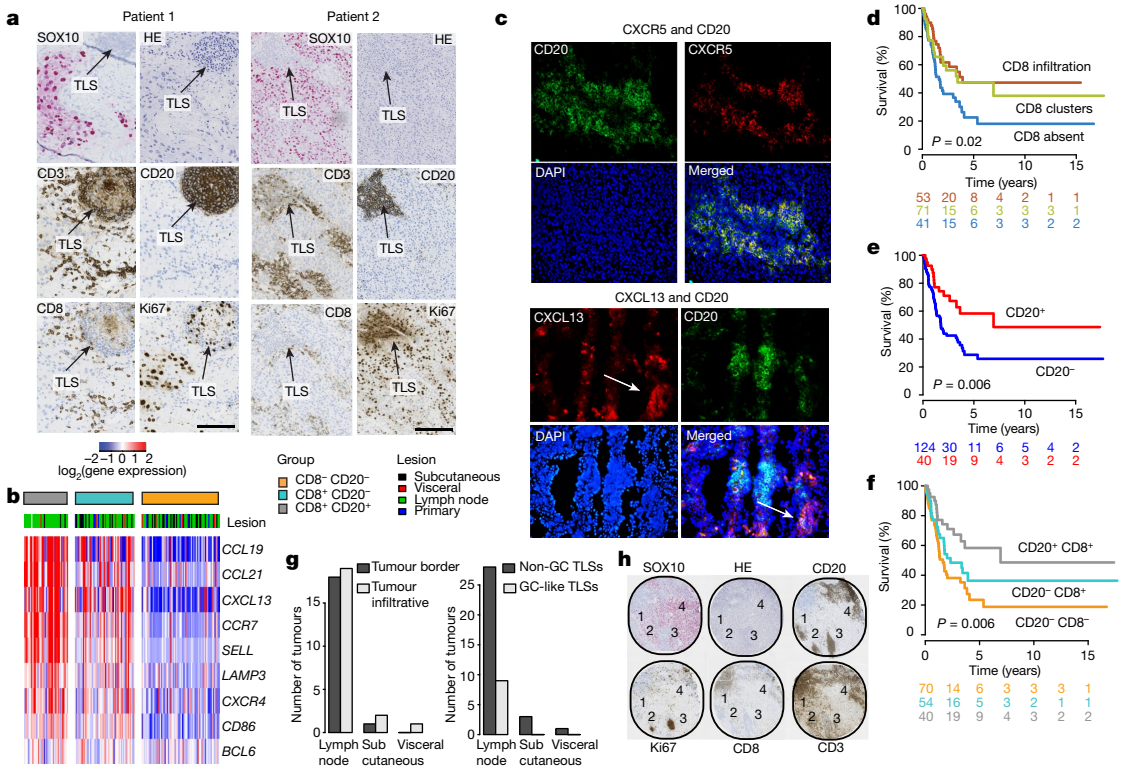

Fig. 1 | Identification of CD20$^+$ B cell clusters in melanoma tumours. **a**, Representative immunostaining of CD20 (B cells), Ki67 (proliferating cells), SOX10 (melanoma cells), CD3 (T cells) and CD8 (T cells). In total, 177 melanoma specimens—including 113 lymph node metastases, 35 subcutaneous metastases, 10 visceral metastases and 15 primary tumours—were analysed. Sections were taken consecutively to spatially analyse the different immunostainings. Scale bars, 100 µm (patient 1), 200 µm (patient 2). HE, haematoxylin and eosin stain. **b**, Gene-expression heat map of known TLS marker genes. The gene-expression data were obtained from matched tumour tissue (n = 160), as was used for the immunostaining. **c**, Representative immunofluorescence staining of CD20 (green) in combination with CXCR5 (red) or CXCL13 (red) in a melanoma tumour known to have TLSs, selected from the immunostaining cohort in **a**. Arrows indicate a CXCL13$^+$ cell cluster. **d**–**f**, Kaplan–Meier survival analysis of the cohort stratified by CD8 (**d**), CD20 (**e**) and combining these two markers (**f**); n = 165, n = 164 and n = 164 patients with available follow-up information in **d**, **e** and **f**, respectively. Cox regression analysis was used to calculate P values. Numbers below plots represent numbers of patients. **g**, TLSs were evaluated for the level of maturation using Ki67 immunostaining and spatial location. Mature germinal-centre (GC)-like structures were detected exclusively in TLSs located in lymph node metastases, and there was no difference in spatial location between lymph node metastases and others. **h**, A representative case with multiple TLSs (numbered 1–4). TLS 2 and TLS 3 show a germinal-centre-like structure within the TLS, whereas TLS 1 and TLS 4 lack these structures. The representative case was selected from n = 18 investigated cases with multiple TLSs.

subsequently lead to chronic inflammation, which is characterized by infiltrating immune cells and generation of TLSs[12]. Importantly, because all tumours with TLSs had tumour-associated CD8$^+$ T cells (Fig. 1a, Extended Data Table 1), we hypothesized that TLSs may support the activation of CD8$^+$ T cell attack against tumour cells. Indeed, survival analysis revealed that the presence of tumour-associated CD8$^+$ T cells or TLSs was associated with improved patient outcome in uni- and multivariate analyses (Fig. 1d, e, Extended Data Table 2). The combination of both TLSs and CD8$^+$ T cells was associated with the best survival outcome, CD8$^+$ T cells alone was linked with intermediate survival, and the absence of both TLSs and CD8$^+$ T cells was associated with the worst survival outcome (Fig. 1f). The survival association of the TLS/CD8$^+$ group was sustained in multivariate analysis adjusting for disease stage, metastasis localization, age and gender (P = 0.006, multivariate Cox regression model) (Extended Data Fig. 1b, Extended Data Table 2). Transcriptomic data showed additional differences in immunological gene signatures[13] (Extended Data Fig. 1c). Although TLSs were not restricted to lymph node metastases, these metastases represented the most-prevalent sample site containing TLSs (Extended Data Fig. 1d, Extended Data Table 1). To further understand the role of TLSs in tumours, we determined the spatial location of TLSs (on the tumour border or infiltrating), the number of TLSs per square millimetre and the presence of germinal-centre-like structures within TLSs using Ki67 immunostaining (Fig. 1g, h). The location of the TLS was independent of metastatic site and, notably, tumours with infiltrative TLSs had a significantly higher frequency of melanomas with a tumour-infiltrative CD8$^+$ T cell pattern (P = 0.009, Fisher's exact test). Using survival analysis of patients with regional lymph node metastases, we found a trend for patients with tumour-infiltrative TLSs having improved survival (Extended Data Fig. 1e). In total, 44% of cases with TLS had multiple TLSs per square millimetre, and these were found only in lymph node metastases (Extended Data Fig. 1f). Moreover, we found nine cases in which canonical germinal-centre-like structures were present within TLSs (Fig. 1g). Importantly, we found cases in which TLSs containing germinal-centre-like structures coexisted with loose, non-germinal-centre-like TLSs in the same tumour (Fig. 1h). The presence in the tumour of TLSs with germinal-centre-like structures was not associated with patient outcome or the CD8$^+$ T cell infiltration pattern. In all, these data support the notion that different types of TLSs exist in individual tumours and that this is independent of the spatial location of the TLS. To reveal the molecular properties of the different T cell, B cell and tumour cell populations, we used the GeoMx digital spatial profiler (Nanostring) to perform high-plex proteomic analysis (Extended Data Table 3) with spatial resolution[14] (Extended Data Fig. 2a). GeoMx data from CD20$^+$ B cell populations localized in TLSs revealed two main groups, characterized by high or low expression

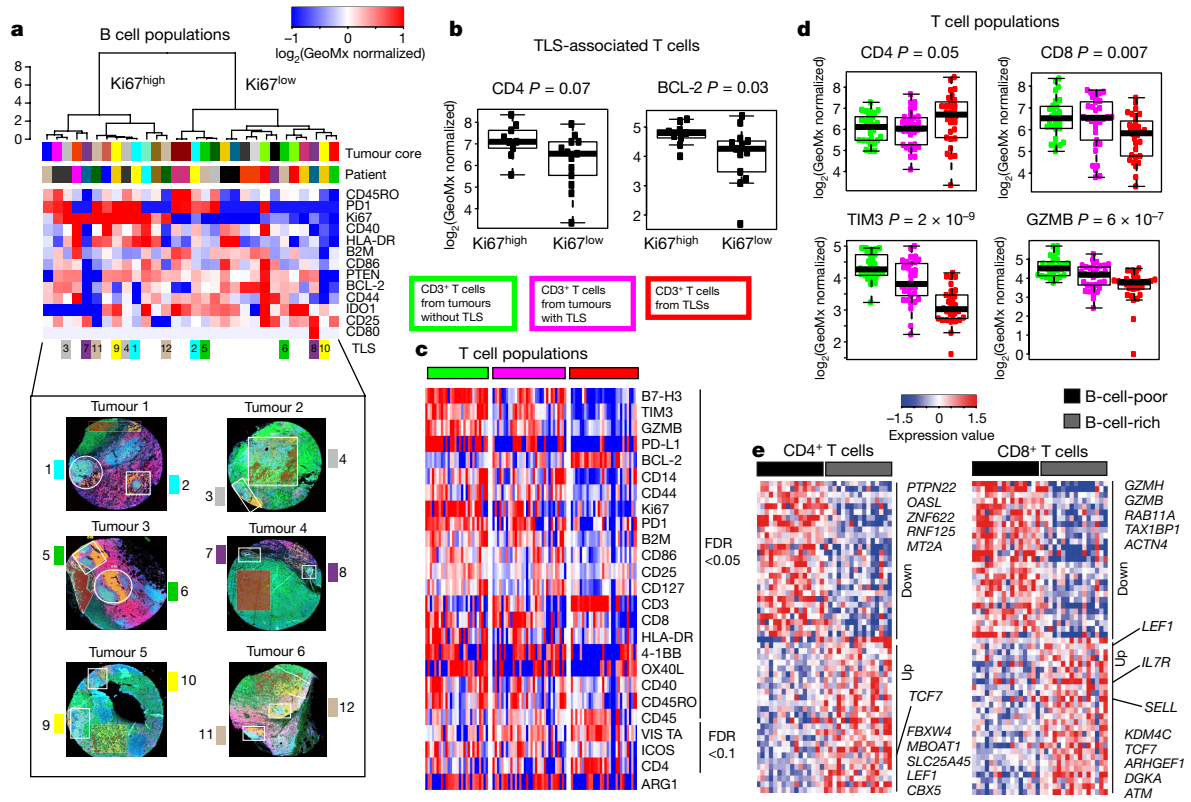

Fig. 2 | B cell heterogeneity and T cell phenotypes using high-plex proteomic and scRNA-seq data. a, Unsupervised hierarchical clustering of B cell populations ($n = 30$) from TLSs across 17 melanoma tumours. Two groups, which were independent of tumour core and patient, were clearly discerned on the basis of Ki67 expression. Proteins were filtered on the basis of scRNA-seq data[18]. Proteins the genes for which were expressed in B cells were included, and those genes not expressed in single B cells were excluded. **b**, T cell populations ($n = 22$) in or in close proximity to Ki67^{high} or Ki67^{low} B cell populations, respectively, were analysed for differences. Box plots of CD4 and BCL-2 show increased expression in T cells located in proximity to Ki67^{high} B cells. *P* value from two-sided Wilcoxon rank-sum test. **c**, **d**, Differential analysis of T cell populations ($n = 91$) from 43 melanoma tumours. Proteins were filtered on the basis of a false-discovery rate (FDR) cut-off. FDR (Benjamini–Hochberg adjustment) from *P* values of Kruskal–Wallis test. Box plots of selected proteins with differential expression. **e**, scRNA-seq data of CD4$^+$ and CD8$^+$ T cells in B-cell-rich and -poor tumours, respectively[17]. Heat map displays tumour means of 27 up- and downregulated genes, as ranked by FDR from a two-sided *t*-test. B-cell-poor ($n = 16$) and -rich ($n = 16$) tumours are defined as those in the lower and upper tertiles, respectively, in terms of the percentage of total cells that are B cells (<1% and >5.3%, respectively). The most significant and relevant genes are highlighted. In the box plots, the centre line is the median, the box limits are the lower and upper quartiles, and the whiskers extend to the most extreme values within 1.5× the interquartile range (IQR).

of Ki67 (Fig. 2a, Extended Data Fig. 2b). Indeed, highly proliferating B cells may operate in germinal centres: the Ki67^{high} tumour-associated B cells that were additionally characterized by increased CD40 expression may therefore belong to more mature TLSs[15]. The data provide further support for the idea that TLSs at different stages exist in the same tumour (Fig. 2a). T cells found in, or in close proximity to, TLSs with Ki67^{high} B cells tended to have a higher proportion of CD4$^+$ cells and increased expression of BCL-2 (Fig. 2b). These T cells may therefore have undergone antigen activation that subsequently led to the upregulation of the pro-survival anti-apoptotic molecule BCL-2[16]. Collectively, these data support the hypothesis that these B cells and T cells belong to mature TLSs. To understand the effect of TLSs on the intratumoral T cell landscape, we analysed different properties of T cells obtained from within or in close proximity to TLSs, infiltrating T cells in tumours with TLSs and T cells from tumours without TLSs. We found increased CD4 and decreased CD8 expression in T cells from within, or in close proximity to, TLSs (Fig. 2c, d). In addition, T cells in tumours without TLSs had increased expression of TIM3, PD1 and GZMB and decreased expression of BCL-2 (Fig. 2c, d). This is consistent with a recent study that demonstrates that T cells in patients who were not responding to immune checkpoint blockade (ICB) had a dysfunctional molecular phenotype[17]. These findings also suggest that distinct patterns of intratumoral adaptive immune activation exist, and that these patterns may partly be driven by TLSs. We then investigated the expression of immune markers on captured tumour cell populations. The largest difference was found when comparing tumours without an immune cell presence to other tumours. As expected, the loss of antigen presentation—via B2M and HLA-DR and decreased PDL1 expression—was found in tumours without an immune cell presence (Extended Data Fig. 2c). However, there was no difference in PDL1 expression in tumour cells between tumours with TLSs and tumours with T cells alone. We further confirmed the loss of B2M protein using immunostaining, and found that protein loss was associated with increased frequency of DNA copy number loss at the *B2M* gene locus. Moreover, we confirmed the loss of MHC using the transcriptomic data. Notably, the inflammatory state and presence of TLSs was not associated with tumour mutational burden or any specific driver-gene mutation (Extended Data Fig. 2d–g).

To gain a deeper molecular understanding of the tumour-associated B cells, we used single-cell RNA-sequencing (scRNA-seq) data. After extracting all B cells from 27 melanoma tumours used in a previous study[18] we then used gene sets to define activated, immature and memory B cells[19], as well as plasma cells[19,20]. We found transcriptional evidence that a mixture of activated and immature B cells, and only a small fraction of plasma cells, are present in melanoma tumours (Extended Data Fig. 3a), which provides further support for the presence of TLSs. A fraction of single B cells expressed the class-switching and affinity

maturation gene *AICDA* or the master regulator of germinal-centre initiation, *BCL6*[15]. Moreover, genes important for germinal-centre initiation (*IRF4*, *POU2AF1*, *MEF2C*, *MYC*, *MEF2B*, *IRF8*, *BCL6*, *MCL1*, *TCF3*, *EBF1*, *SPIB*, *DOCK8* and *BACH2*), the germinal-centre light zone (*CD83* and *CD86*) the germinal-centre dark zone (*CXCR4*), and T cell interaction (*CD40*) were abundantly expressed in B cells[15] (Extended Data Fig. 3b). Thus, the transcriptional data suggest a wide range of B-cell-derived, immature-to-mature germinal-centre signals. This is consistent with the heterogeneity of TLS states observed in the immunostaining and GeoMx data. MHC class I and II molecules displayed a uniform high expression across single B cells, which suggests that B cells within TLSs are generally capable of antigen presentation. The expression of *IGLL1*, a component of the B cell receptor in pre-B cells displayed an intriguing pattern. Three clear B cell groups could be discerned; plasma cells, cells positive for *IGLL1* and *IGLL5* and cells negative for *IGLL1* and *IGLL5*. These groups could be further subdivided on the basis of *CD69* expression (Extended Data Fig. 3b). Using previously published scRNA-seq data[17], we found that the fraction of $CD69^+$ and $IGLL5^-$ $CD69^+$ cells—and not $IGLL5^+$ B cells—was associated with the response to ICB (Extended Data Fig. 3c). Moreover, the $CD69^+$ B cell group we identified presents a more-pronounced germinal-centre-reaction phenotype than the $IGLL1^+$ $IGLL5^+$ B cell group, as CD69 is correlated with markers of the mature germinal centre such as CD83 and CXCR4 (Extended Data Fig. 3d). Therefore, the observed B cell groups may reflect the maturation state of the underlying germinal-centre reaction that occurs in TLSs. By contrast, the percentage of $IGHD^+$ B cells ('unswitched' IgD^+) and $IGHG^+$ B cells ('switched' IgG^+) were not predictive of therapy outcome at baseline (Extended Data Fig. 3c). Collectively, these data support the presence of distinct subsets of B cells at different stages of B cell development, and their role in the response to ICB; however, further studies are needed to confirm the role of $CD69^+$ B cells. Finally, we investigated whether the immune microenvironment of the tumour is adapted by the presence of B cells. In single-cell data, B-cell-rich samples contained more $CD4^+$ and $CD8^+$ T cells with naive and/or memory-like characteristics (expressing *TCF7* and *IL7R*) as compared to B-cell-poor samples (Fig. 2e), suggesting an influx of naive and memory T cells to TLSs. Such memory $TCF7^+$ T cells have previously been associated with an improved response to ICB[17]. This is consistent with our GeoMx data, in which T cells in tumours without TLSs had an exhausted-like molecular phenotype (Fig. 2c).

Next, we used differential expression analysis to create a gene signature that reflects melanoma tumours with TLSs (Fig. 3a, Extended Data Table 4). This signature included known B-cell-specific genes such as *CD79B*. Another interesting candidate is *CCR6*, which was recently found to be upregulated in activated B cells[21]. Indeed, in the single-cell data from melanomas[17,18], *CCR6* and *CD79B* are specifically expressed in tumour-associated B cells. The remaining genes of the signature were expressed mainly by other types of immune cell (Extended Data Fig. 3e). Similarly, the TLS-hallmark genes *CCR7*, *CXCR5* and *SELL* (which encodes CD62L) were expressed in single B cells and—to some degree—by $CD4^+$ T cells, whereas *CXCL13* is expressed predominantly by $CD8^+$ T cells (Extended Data Fig. 3f). This suggests that TLSs localized in melanoma tumours consist of B cells and other immune cells. Next, we constructed a signature from a compendium of TLS-hallmark genes (*CCL19*, *CCL21*, *CXCL13*, *CCR7*, *CXCR5*, *SELL* and *LAMP3*)[11], and found that it correlates closely with our TLS signature in three datasets[22–24] (correlations of 0.91, 0.85 and 0.87). Further, the TLS signature correlated strongly with B cell signatures and single B cell markers. The TLS signature also correlated with signatures of T cells and other types of immune cell[25,26]—although not to the same extent as it did to B cell signatures (Extended Data Fig. 4a). To gain further support for the TLS signature we derived, we retrieved RNA-seq data for metastatic melanomas from The Cancer Genome Atlas (TCGA) project[24]. Trichotomizing the data on the basis of our TLS signature confirmed the association with patient survival (Fig. 3b, Extended Data Table 2). Analysis of matched mutation data revealed no difference in mutational burden (Fig. 3c). Notably, samples with a TLS^{high} signature also included non-lymph-node metastases, and—when extended to primary tumours—a small portion of the primary tumours also had a high TLS gene score (Extended Data Fig. 4b). Collectively, this confirms a prognostic role for TLS in melanoma.

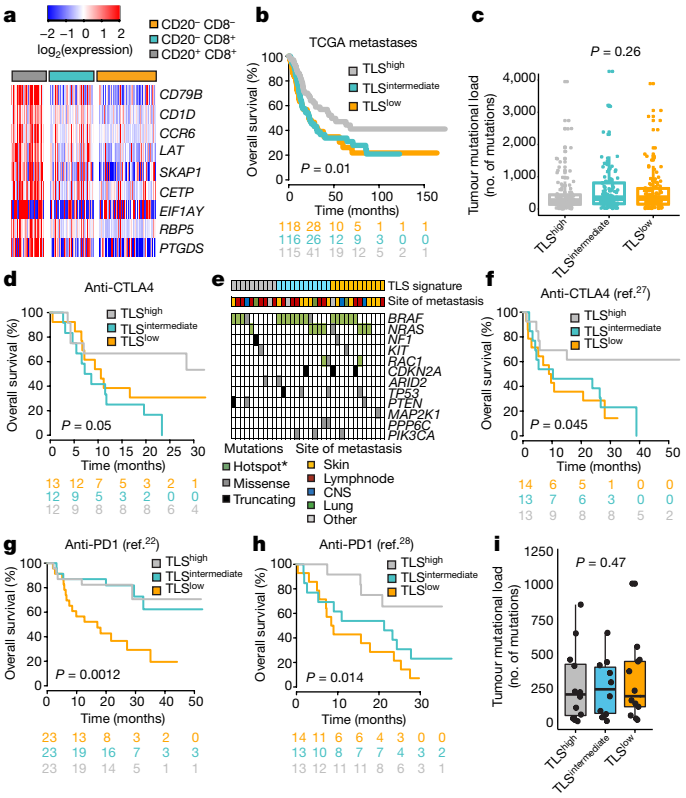

Fig. 3 | TLS gene signature derived from the $CD8^+CD20^+$ group predicts prognosis and response to ICB in melanoma. a, Heat map of genes specifically upregulated in $CD8^+CD20^+$ cases of melanoma. **b**, Kaplan–Meier analysis based on the trichotomized TLS gene signature in the melanoma metastases cohort from the TCGA ($n = 349$ patients with available follow-up information). *P* value from Cox regression analysis. **c**, Mutational load across TCGA TLS groupings in **b**. *P* value from Kruskal–Wallis test. **d**, Kaplan–Meier analysis for overall survival in patients treated with anti-CTLA4 ($n = 37$). *P* value from Cox regression analysis. **e**, Mutational pattern in patients treated with anti-CTLA4. **f**, Kaplan–Meier analysis for overall survival in patients treated with anti-CTLA4 ($n = 40$). *P* value from Cox regression analysis. Data from a previous study[27] were used. **g**, Kaplan–Meier analysis for overall survival in patients treated with anti-PD1 ($n = 69$). *P* value from Cox regression analysis. Data from a previous study[22] were used. **h**, Kaplan–Meier analysis for overall survival in patients treated with anti-PD1 ($n = 40$). *P* value from Cox regression analysis. Data from a previous study[28] were used. **i**, Mutational load across the TLS grouping, using data from a previous publication[28]. *P* value from Kruskal–Wallis test. In **b**, **d**, **f**–**h**, patients were trichotomized according to high, intermediate and low expression of the TLS signature score. In the box plots, centre line is the median, the box limits are the lower and upper quartiles, and the whiskers extend to the most extreme values within 1.5× IQR. Numbers below plots represent numbers of patients.

Given the success of ICB in treating melanoma, we investigated the importance of tumour-associated TLSs in response to therapy (Extended Data Table 5). First, we gathered a collection of melanoma tumour biopsies from patients who were receiving CTLA4 blockade. Trichotomizing gene-expression data on the basis of the TLS signature revealed that TLS^{high} tumours in particular were associated with significantly increased survival after CTLA4 blockade (Fig. 3d, Extended Data Fig. 5a, Extended Data Table 2). Mutation data in melanoma driver genes further supported the notion that the TLS signature is independent of tumour genetic mechanisms (Fig. 3e). We further verified the predictive

effect of the TLS signature using previously published[27] data from an additional cohort of 40 patients with melanoma who were receiving CTLA4 blockade (Fig. 3f). Previous studies have demonstrated tumour mutational burden as a predictive biomarker for response to ICB[28]. However, in this cohort of patients treated with anti-CTLA4, the TLS signature is independent of mutational load (Extended Data Fig. 5b). Moreover, the TLS signature was significantly associated with overall survival in a previously published[22] dataset of pretreatment samples from 69 patients who were undergoing anti-PD1 monotherapy or anti-CTLA4 and anti-PD1 combination therapy (Fig. 3g). We also observed the predictive effect of the TLS signature in a previously published[28] dataset of pretreatment samples from 41 patients who were treated with anti-PD1 (of whom 50% had been exposed to anti-CTLA4 before anti-PD1 treatment) (Fig. 3h, Extended Data Fig. 5c). Finally, we performed meta Cox regression analysis across the four cohorts treated with ICB, using multiple immune signatures: of these, our TLS signature performed best (Extended Data Fig. 5D). The TLS signature was also independent of tumour mutational load in the cohort treated with anti-PD1 (Fig. 3i), consistent with previous studies that have shown that immune gene signatures are not correlated with mutational load[29]. Although we did not observe significant differences in the TLS gene-expression score retrieved from pretreatment biospies with regards to 'response evaluation criteria in solid tumours' (RECIST), we observed a notable difference in RNA-seq data from on-treatment biopsies that were collected on cycle 1 at day 29, which was confirmed in previously published cases of patients treated with anti-PD1[30] (Extended Data Fig. 5e, f). This indicates that TLS functionality is induced by ICB treatment in patients with a clinical response. To further determine the biological relevance of our TLS signature, we applied it to RNA-seq data from 13 additional samples of melanoma that were obtained from patients who were receiving ICB, and performed concurrent immunostaining of CD20 and CD3. The samples with the highest TLS gene score contained TLSs (as detected by CD20 immunostaining), which confirms the ability of our gene signature to predict samples with TLSs (Extended Data Fig. 5g).

In conclusion, our data provide evidence that TLSs may have a key role in sustaining an immune-responsive microenvironment. This finding opens avenues for therapeutic strategies that aim at enhancing TLS formation and function, which could result in improved clinical outcomes and responses to cancer immunotherapy.

Online content

Any methods, additional references, Nature Research reporting summaries, source data, extended data, supplementary information, acknowledgements, peer review information; details of author contributions and competing interests; and statements of data and code availability are available at https://doi.org/10.1038/s41586-019-1914-8.

1. Robert, C. et al. Pembrolizumab versus ipilimumab in advanced melanoma. *N. Engl. J. Med.* **372**, 2521–2532 (2015).
2. Gopalakrishnan, V. et al. Gut microbiome modulates response to anti-PD-1 immunotherapy in melanoma patients. *Science* **359**, 97–103 (2018).
3. Cristescu, R. et al. Pan-tumor genomic biomarkers for PD-1 checkpoint blockade-based immunotherapy. *Science* **362**, eaar3593 (2018).
4. Ladányi, A. et al. Prognostic impact of B-cell density in cutaneous melanoma. *Cancer Immunol. Immunother.* **60**, 1729–1738 (2011).
5. Messina, J. L. et al. 12-Chemokine gene signature identifies lymph node-like structures in melanoma: potential for patient selection for immunotherapy? *Sci. Rep.* **2**, 765 (2012).
6. Cipponi, A. et al. Neogenesis of lymphoid structures and antibody responses occur in human melanoma metastases. *Cancer Res.* **72**, 3997–4007 (2012).
7. Sautès-Fridman, C., Petitprez, F., Calderaro, J. & Fridman, W. H. Tertiary lymphoid structures in the era of cancer immunotherapy. *Nat. Rev. Cancer* **19**, 307–325 (2019).
8. Petitprez, F. A. d. R et al. B cells are associated with survival and immunotherapy response in sarcoma. *Nature* https://doi.org/10.1038/s41586-019-1906-8 (2020).
9. Helmink, B. A. et al. B cells and tertiary lymphoid structures promote immunotherapy response. *Nature* https://doi.org/10.1038/s41586-019-1922-8 (2020).
10. Mihm, M. C., Jr & Mulé, J. J. Reflections on the histopathology of tumor-infiltrating lymphocytes in melanoma and the host immune response. *Cancer Immunol. Res.* **3**, 827–835 (2015).
11. Dieu-Nosjean, M. C., Goc, J., Giraldo, N. A., Sautès-Fridman, C. & Fridman, W. H. Tertiary lymphoid structures in cancer and beyond. *Trends Immunol.* **35**, 571–580 (2014).
12. Germain, C., Gnjatic, S. & Dieu-Nosjean, M. C. Tertiary lymphoid structure-associated B cells are key players in anti-tumor immunity. *Front. Immunol.* **6**, 67 (2015).
13. Bindea, G. et al. Spatiotemporal dynamics of intratumoral immune cells reveal the immune landscape in human cancer. *Immunity* **39**, 782–795 (2013).
14. Amaria, R. N. et al. Neoadjuvant immune checkpoint blockade in high-risk resectable melanoma. *Nat. Med.* **24**, 1649–1654 (2018).
15. De Silva, N. S. & Klein, U. Dynamics of B cells in germinal centres. *Nat. Rev. Immunol.* **15**, 137–148 (2015).
16. Rogers, P. R., Song, J., Gramaglia, I., Killeen, N. & Croft, M. OX40 promotes Bcl-xL and Bcl-2 expression and is essential for long-term survival of CD4 T cells. *Immunity* **15**, 445–455 (2001).
17. Sade-Feldman, M. et al. Defining T cell states associated with response to checkpoint immunotherapy in melanoma. *Cell* **175**, 998–1013 (2018).
18. Jerby-Arnon, L. et al. A cancer cell program promotes T cell exclusion and resistance to checkpoint blockade. *Cell* **175**, 984–997 (2018).
19. Angelova, M. et al. Characterization of the immunophenotypes and antigenomes of colorectal cancers reveals distinct tumor escape mechanisms and novel targets for immunotherapy. *Genome Biol.* **16**, 64 (2015).
20. Tarte, K., Zhan, F., De Vos, J., Klein, B. & Shaughnessy, J. Jr. Gene expression profiling of plasma cells and plasmablasts: toward a better understanding of the late stages of B-cell differentiation. *Blood* **102**, 592–600 (2003).
21. Suan, D. et al. CCR6 defines memory B cell precursors in mouse and human germinal centers, revealing light-zone location and predominant low antigen affinity. *Immunity* **47**, 1142–1153 (2017).
22. Gide, T. N. et al. distinct immune cell populations define response to anti-PD-1 monotherapy and anti-PD-1/anti-CTLA-4 combined therapy. *Cancer Cell* **35**, 238–255 (2019).
23. Cirenajwis, H. et al. NF1-mutated melanoma tumors harbor distinct clinical and biological characteristics. *Mol. Oncol.* **11**, 438–451 (2017).
24. Cancer Genome Atlas Network. Genomic classification of cutaneous melanoma. *Cell* **161**, 1681–1696 (2015).
25. Becht, E. et al. Estimating the population abundance of tissue-infiltrating immune and stromal cell populations using gene expression. *Genome Biol.* **17**, 218 (2016).
26. Tirosh, I. et al. Dissecting the multicellular ecosystem of metastatic melanoma by single-cell RNA-seq. *Science* **352**, 189–196 (2016).
27. van Allen, E. M. et al. Genomic correlates of response to CTLA-4 blockade in metastatic melanoma. *Science* **350**, 207–211 (2015).
28. Riaz, N. et al. Tumor and microenvironment evolution during immunotherapy with nivolumab. *Cell* **171**, 934–949 (2017).
29. Lauss, M. et al. Mutational and putative neoantigen load predict clinical benefit of adoptive T cell therapy in melanoma. *Nat. Commun.* **8**, 1738 (2017).
30. Roh, W. et al. Integrated molecular analysis of tumor biopsies on sequential CTLA-4 and PD-1 blockade reveals markers of response and resistance. *Sci. Transl. Med.* **9**, eaah3560 (2017).

Methods

No statistical methods were used to predetermine sample size. The experiments were not randomized and investigators were not blinded to allocation during experiments and outcome assessment.

Patient material

This study was approved by the Regional Ethics Committee at Lund University (Dnr. 191/2007 and 101/2013). The sample cohort, representing a population-based retrospective collection ($n = 177$), was obtained at the Department of Surgery at Skåne University Hospital.

Overall, 104 patients had regional metastatic disease, 50 distant disease and 19 local disease. Four patients were of unknown stage. This is a historical cohort, collected between 2000 and 2012. As such, the cohort is suitable for prognostic studies. A summary of the patient characteristics is provided in Extended Data Table 1.

We also collected paraffin-embedded tumour tissue from 119 patients; 37 of these patients had received anti-CTLA4 as first-line therapy. Tumour tissue was collected from these patients in Denmark, and available biopsies were obtained a maximum of six months before the start of therapy. This study was approved by the regional ethical committee (H-15010200). DNA and RNA were extracted using the Qiagen FFPE AllPrep procedure, as previously described[31].

We retrieved frozen tumour tissue from 13 patients who were undergoing anti-PD1 therapy at Skåne University Hospital, under ethical approval Dnr. 101/2013. RNA-seq and data analysis was performed as previously described[29].

High-plex proteomic analysis

We used the Nanostring GeoMx platform for high-plex proteomic analysis with spatial resolution, as previously described[14]. Two 5-µm tissue microarray slides were used. Antibodies against CD3, CD20, DAPI, and PMEL and S100B were used for immunofluorescence, which was subsequently used for region of interest selection and UV masking. Digital counts from barcodes corresponding to protein probes (in total 60 immune-related proteins) were analysed as follows: raw counts were first normalized with internal spike-in controls (ERCC) to account for system variation. To control for nonspecific antibody binding, values were further normalized by a linear scaling factor to obtain IgG control counts of 1 for each region of interest. To reduce background noise, values below 3 were set to 1 and the data were $\log_2$-transformed. Data are provided in Supplementary Information.

Immunohistochemistry

Tissue microarrays were constructed using, on average, three 1-mm cores per tumour in an attempt to obtain a representative picture of the tumour. The tissue block was cut in 4-µm sections, and then dried at 60 °C for 1 h. The paraffin-embedded sections were deparaffinized and pretreated in the PT-Link (DAKO) with target retrieval solution buffer pH 9. The following steps (except for the primary antibody staining) were performed in the DAKO staining equipment (Autostainer plus) with DAKO kit K8010 solutions: peroxidase block (5 min), EnVision HRP-conjugated polymers (30 min), DAB substrate–chromogen solution (2 × 5 min) and counterstaining with haematoxylin (4 min). Between each step, the sections were rinsed with washing buffer. Finally, the sections were dehydrated and mounted with PERTEX mounting medium (ref. 00811) (Histolab). The primary antibodies used were all from Agilent/DAKO: CD3 (A0452) in 1:200 dilution, CD8 (M7103) in 1:100 dilution, MITF (Clone C5), B2M (A0072), Ki67 (MIB-1) in 1:500 dilution and CD20 (M0755) in 1:400 dilution. SOX10 was performed in the clinical routine laboratory of clinical pathology (Skåne University Hospital) using the mouse monoclonal IgG1 (clone BC34, Biocare Medical) antibody.

Immunofluorescence staining

Initially, the cells from snap-frozen tumours known to have TLSs were incubated in ice-cold acetone for 10 min and washed in PBS. All the following steps were performed in a humidified chamber. Unspecific binding sites were masked with PBS + 3% BSA for 90 min at room temperature. Mouse-anti-CD20 (1:200, 00064779, DAKO), rabbit-anti-CXCR5 (1:200, 3180237-9, Abcam) and rabbit-anti-CXCL13 (1:200, NBP2-1604155, Novus Biologicals) were applied overnight at 4 °C. Donkey-anti-mouse-AF488 and goat-anti-rabbit-AF546 was applied 1:1,000 in PBS + 1% BSA for 90 min at room temperature, followed by mounting with DAPI-containing mounting medium (Vector Laboratories). Fluorescence images were acquired with an Olympus BX63 microscope, DP80 camera and cellSens Dimension v.1.12 software (Olympus).

Bioinformatic and statistical analyses

Datasets. Microarray expression data were generated using the Illumina HT12 arrays, and have been used in a previous publication[23]; they are deposited in Gene Expression Omnibus, accession number GSE65904. Mutation data were generated using a sequencing panel targeting 1,550 cancer genes, as previously described[23], and copy number data were derived from the corresponding raw sequencing data using Contra version 2.0.3[32] with segmentation using GLAD[33].

RNA-seq data of metastatic melanomas from TCGA (level 3, release 3.1.14.0) were downloaded from the data portal, quantile-normalized and log-transformed as $\log_2(\text{data} + 1)$.

The PD1-treatment RNA-seq data from ref. [22] were downloaded as fastq files from the European Nucleotide Archive (PRJEB23709) and fragments per kilobase of transcript per million mapped reads (FPKM) values were retreived using HISAT and Stringtie[34]. The data were reduced to protein-coding genes, samples were quantile-normalized and the data were log-transformed as $\log_2(\text{data} + 1)$. Previously published PD1 inhibitor-treatment RNA-seq data[28] were downloaded as count data ('CountData.BMS038.txt') with annotations from https://github.com/riazn/bms038_analysis/tree/master/data. The data were reduced to protein-coding genes and normalized for transcript lengths using exon annotations from the R package TxDb.Hsapiens.UCSC.hg19.knownGene, subsequently transformed to transcripts per million (TPM) and quantile-normalized. The data were log-transformed as $\log_2(\text{data} + 2) - 1$. Previously published NanoString gene-expression data[30] were downloaded from the respective supplementary table. Previously published CTLA4 inhibitor-treatment data[27] were received from the authors as reads per kilobase of transcript per million mapped reads (RPKM) values; the data were quantile-normalized and log-transformed as $\log_2(\text{data} + 1)$. scRNA-seq data were retrieved from Gene Expression Omnibus accessions GSE115978 and GSE120575, protein-coding genes were kept and cells with less than 1,700 or 1,000 genes expressed >0 were removed, respectively. Data for B cells were extracted, and quantile-normalized. For GSE115978, the available B cell definition was used; for GSE120575, no B cell definition was available and B cells were defined as CD19 > 2.

We generated gene-expression profiles from 119 formalin-fixed paraffin-embedded (FFPE) samples using Affymetrix Clariom D microarrays. The hybridized FFPE material constituted three separate retrospective studies, including the 37 pre-ipilimumab treatment samples analysed in this study. Principal component (PC) analysis informed us that this FFPE-derived data was greatly affected by sample degradation. We therefore reduced the data to probesets mapping to the 3′ untranslated region (UTR) of curated RefSeq transcripts; using PRINCIPAL categories from APPRIS[35], we obtained 33,111 probesets in the 3′ UTRs of the principal gene isoforms. We further selected the two cohorts from the same Danish site, and removed one sample with a sample median expression < 0 and 7 samples with a median control exon ('HTA2-pos' probes) minus median control intron ('HTA2-neg' probes) expression < 1. The remaining probesets were filtered for being expressed, by keeping probesets that were above the median control intron expression in at least 90% of samples (19,990 probesets). The most-varying probeset for each protein-coding gene was kept (10,197 genes), and quantile

normalization was applied. As the data was still affected by degradation, PC1 and PC2 of the data were removed using R package swamp[36], an offset of 1.5 was added to revert negative values, and the 5,000 genes with the largest variation were kept. Gene-expression data of the 37 samples of cutaneous melanoma with ipilimumab pretreatment were extracted for this study (Supplementary Information). Additional data and codes are available from the corresponding author upon request.

TLS signature. To derive the TLS-signature genes, we performed SAM analysis[37] to identify genes overexpressed in $CD8^+CD20^+$ versus $CD8^+$ groups and subtracted the genes overexpressed in $CD8^+$ versus double-negative groups (Extended Data Table 4). For each dataset, the signature genes that were present were extracted. Failed genes were defined as having an average Pearson correlation <0.15 to the other signature genes, and were excluded. The signature score was calculated as the mean gene expression. For survival analyses, the signature score was divided into equally sized tertiles.

Statistical analyses. Fisher's exact test was used for comparison of categorical variables. Pearson correlation was used for comparison of numerical variables. The *t*-test or Wilcoxon test and analysis of variance (ANOVA) were used for group comparisons of two or more than two groups, respectively. Owing to outliers, we used the Kruskal–Wallis test for the association of mutational load with the immunohistochemical groups. For univariate and multivariate survival analyses, we used Cox regression from the survival package. All bioinformatical analyses were done in R. All tests were two-sided. All box plots are depicted with the centre line representing the median, the box limits representing the lower and upper quartiles, and the whiskers extending to the most extreme values within 1.5× IQR.

Reporting summary

Further information on research design is available in the Nature Research Reporting Summary linked to this paper.

Data availability

All relevant data are available and are included as Source Data. Digital spatial-profiling data used in Fig. 2 and gene-expression microarray data from Danish patients treated with anti-CTLA4 are available as Source Data. Data from public repositories were accessed from GSE65904 (ref. [23]), TCGA data portal SKCM level 3 release 3.1.14.0, PRJEB23709 (ref. [22]), https://github.com/riazn/bms038_analysis/tree/master/data, GSE115978 (ref. [18]) and GSE120575 (ref. [17]). Any other relevant data and code can be obtained from the corresponding authors upon reasonable request.

31. Harbst, K. et al. Molecular profiling reveals low- and high-grade forms of primary melanoma. *Clin. Cancer Res.* **18**, 4026–4036 (2012).
32. Li, J. et al. CONTRA: copy number analysis for targeted resequencing. *Bioinformatics* **28**, 1307–1313 (2012).
33. Hupé, P., Stransky, N., Thiery, J. P., Radvanyi, F. & Barillot, E. Analysis of array CGH data: from signal ratio to gain and loss of DNA regions. *Bioinformatics* **20**, 3413–3422 (2004).
34. Pertea, M., Kim, D., Pertea, G. M., Leek, J. T. & Salzberg, S. L. Transcript-level expression analysis of RNA-seq experiments with HISAT, StringTie and Ballgown. *Nat. Protocols* **11**, 1650–1667 (2016).
35. Rodriguez, J. M. et al. APPRIS: annotation of principal and alternative splice isoforms. *Nucleic Acids Res.* **41**, D110–D117 (2013).
36. Lauss, M. et al. Monitoring of technical variation in quantitative high-throughput datasets. *Cancer Inform.* **12**, 193–201 (2013).
37. Tusher, V. G., Tibshirani, R. & Chu, G. Significance analysis of microarrays applied to the ionizing radiation response. *Proc. Natl Acad. Sci. USA* **98**, 5116–5121 (2001).

Acknowledgements The study was supported by the Swedish Cancer Society, the Swedish Research Council, BioCARE, the Berta Kamprad Foundation, the King Gustaf V Jubilee foundation, Mats Paulsson's foundation, Stefan Paulsson's foundation and governmental funding for healthcare research (ALF). The Danish Cancer Society, the Aase and Einar Danielsen's Fund and the Capital Region of Denmark Research Foundation. This project has received funding from the European Union's Horizon 2020 research and innovation programme under the Marie Skłodowska-Curie grant agreement no. 641458.

Author contributions G.J. conceived and supervised the study. R.C., M.L. and G.J. analysed and drafted text. R.C., B.P., K.L. and K.J. generated immunostaining data. R.C., A.S., I.J., B.P. and G.J. analysed immunostaining data. R.C., K.P. and G.J. generated and analysed immunofluorescence data. A.v.S. and S.W. generated digital spatial-profiling data. M.L. and G.J. analysed digital spatial-profiling data. R.C., M.L., S.M., K.H. and G.J. performed statistical analyses. M.L. and G.J. performed bioinformatic analyses. M.L. analysed scRNA-seq data. J.V.-C. generated RNA-seq data. M.L., A.S., M.D., M.S.L., I.J., B.P., K.H., J.V.-C., A.v.S., K.L., S.W., K.J., K.P., D.S., J.A.W. and G.J. interpreted data. M.D., M.S.L., H.O., C.I., K.I., H.S., L.B., A.C. and I.M.S. collected clinical specimens and clinical data. All authors approved and read the final draft.

Competing interests S.W and A.v.S. are employees of Nanostring Inc. and declare that there are competing interests. All other authors declare no conflict of interest.

Additional information
Supplementary information is available for this paper at https://doi.org/10.1038/s41586-019-1914-8.
Correspondence and requests for materials should be addressed to G.J.
Peer review information *Nature* thanks James J. Mulé, Caroline Robert and the other, anonymous, reviewer(s) for their contribution to the peer review of this work.
Reprints and permissions information is available at http://www.nature.com/reprints.

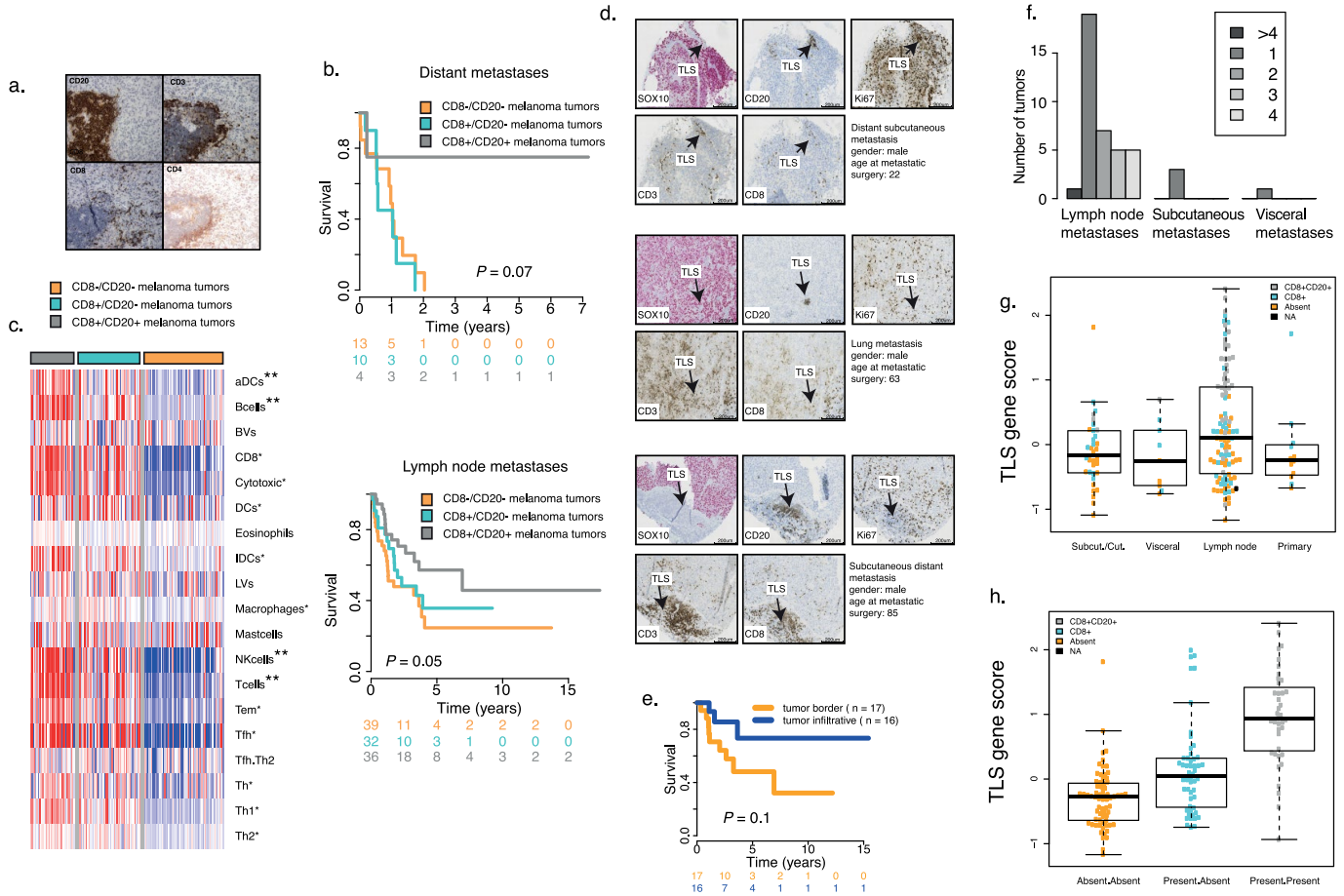

Extended Data Fig. 1 | Characterization of TLSs in melanoma tumours. **a**, CD20 (B cells), CD3 (T cells), CD8 (CD8$^+$ T cells) and CD4 (CD4$^+$ T cells) immunostaining in a representative melanoma with a TLS ($n = 44$ cases with TLS in the cohort of 177 cases). **b**, Subset survival analysis using CD8 and CD20 immunostaining in distant and lymph node metastases separately. $n = 27$ and 97 patients with available follow-up information, respectively. P values from Cox regression. **c**, Gene-expression characterization of the three groups using previously described signatures[13]. aDCs, activated dendritic cells; BVs, blood vessels; DCs, dendritic cells; IDCs, immature dendritic cells; LVs, lymph vessels; NK, NK cells; Tem, T effector memory cells; Tfh, T follicular helper cells; Tfh. Th2, T follicular helper 2 cells; Th, T helper cell; Th1, T helper 1 cell; Th2, T helper 2 cell. **d**, CD20, CD3, CD8, Ki67 and SOX10 immunostainings in three distant metastases. Arrows indicate the TLS. **e**, Survival analysis of 33 patients with TLS-containing tumours from regional lymph node metastases, stratified according to whether the TLS is located at the tumour border or is tumour-infiltrative. P value from Cox regression. **f**, Bar plot showing quantification of TLSs in tumours. Numbers in the box corresponds to TLSs per square millimetre. **g**, TLS gene score and type of lesion. $n = 159$ tumours. **h**, TLS score and immunological group. $n = 159$ tumours. In the box plots, the centre line represents the median, the box limits represent the lower and upper quartiles, and the whiskers extend to the most extreme values within 1.5× IQR. Numbers below the graphs represent numbers of patients.

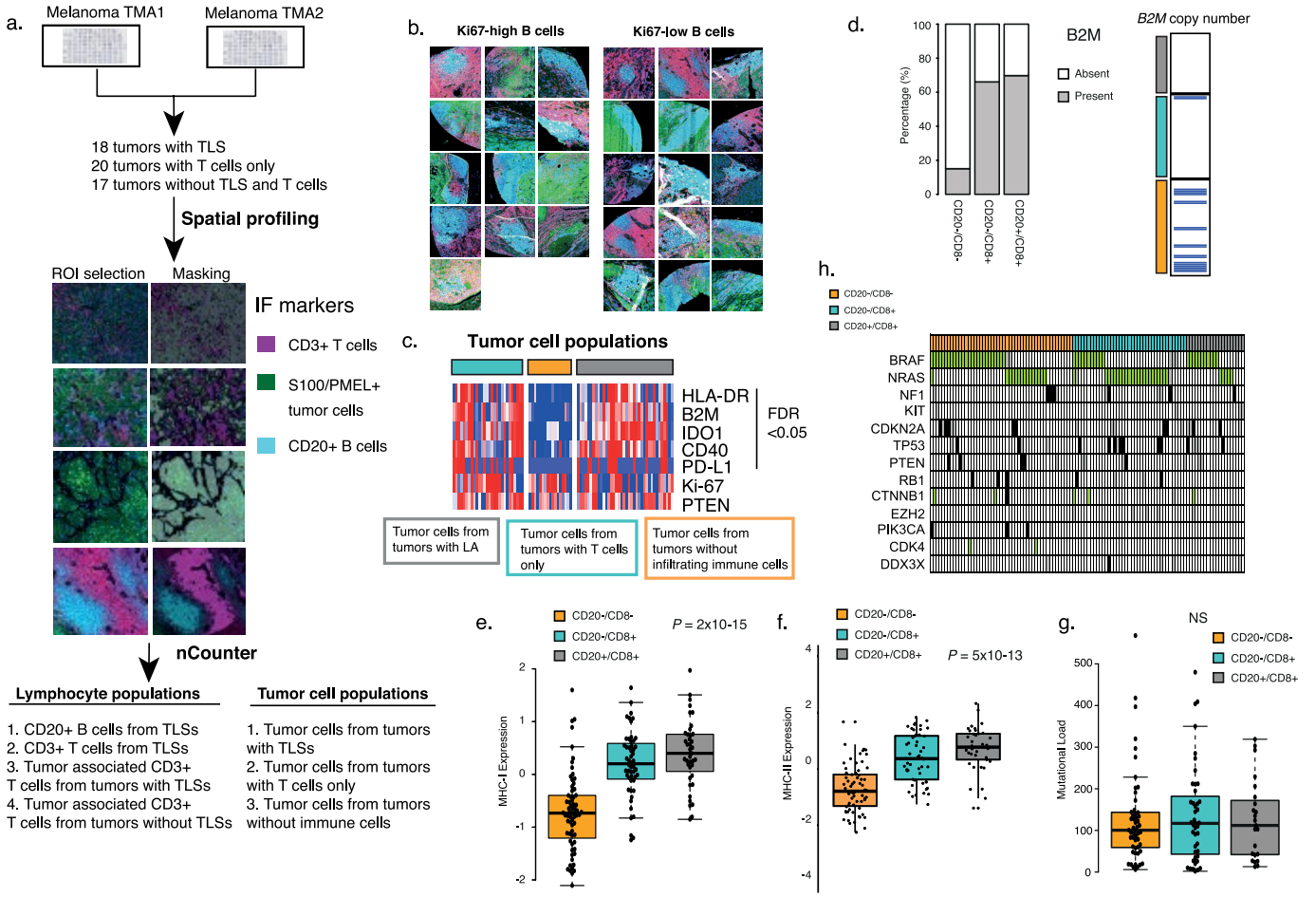

Extended Data Fig. 2 | High-plex proteomic analysis using the GeoMx assay and genomic characterization of tumours containing TLSs. a, Workflow of the GeoMx assay. **b**, Immunofluorescence imaging of TLSs in tumour samples used in the GeoMx analysis. TLSs are sorted according to the unsupervised clustering of the high-plex proteomic data, performed on the different B cell populations. Pink, $CD3^+$ T cells; green, tumour cells positive for PMEL and/or S100B; cyan, $CD20^+$ B cells. For $Ki67^{high}$ 13 of 13 TLSs are displayed, and for $Ki67^{low}$ 15 of 17 TLSs are displayed. **c**, GeoMx data from 83 captured tumour cell regions. FDRs are from Kruskal–Wallis test, adjusted for multiple testing using the Benjamini–Hochberg method. **d**, Left, B2M immunostaining shows a significant difference between CD8/CD20 groups. $P = 1 \times 10^{-11}$, Fisher's exact test, $n = 172$ tumours). Right, plot shows B2M copy number status (blue = loss). $P = 0.002$, FDR adjustment for multiple comparisons = 0.007, Fisher's exact test, $n = 127$ tumours. **e**–**g**, MHC-I (**e**) and MHC-II (**f**) expression ($n = 160$ tumours, P value from ANOVA) and mutational load (**g**) ($n = 118$ tumours, Kruskal–Wallis test) in relation to immunological groupings. **h**, Mutation heat map of melanoma-relevant genes in relation to immunological grouping. In the box plots, the centre line represents the median, the box limits represent the lower and upper quartiles, and the whiskers extend to the most extreme values within 1.5× IQR.

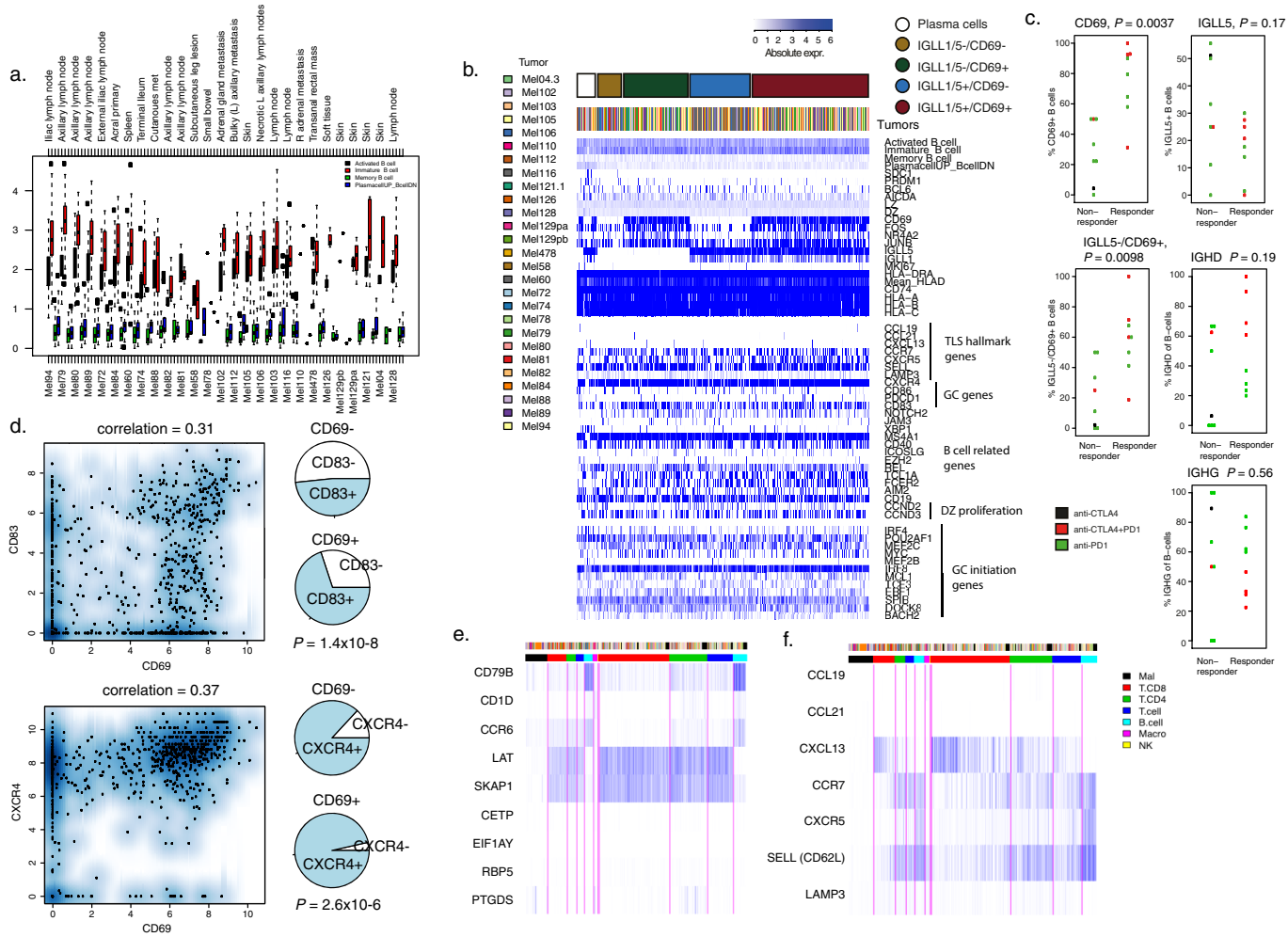

Extended Data Fig. 3 | scRNA-seq analysis of tumour-associated B cells. **a**, Box plots of gene-expression scores, based on different B cell developmental states in 812 B cells from 27 tumours from a previous study[18]. **b**, Heat map of selected genes across all 812 B cells. *IGLL5* and *CD69* were two of the five genes with highest expression variation across all B cells. The heat map is sorted on *IGLL5* and *CD69* expression, excluding the cells that displayed increased expression of the plasma-cell signature. Genes showing a Pearson correlation >0.4 to *IGLL5* or *CD69* expression are also indicated. *SDC1* and *PRDM1* mark plasma cells, *BCL6* and *AICDA* mark germinal centres, *HLA-DRA* mark MHC-II and *HLA-A*, *HLA-B* and *HLA-C* mark MHC-I. TLS-hallmark genes, germinal-centre-related genes and other B cell genes are also indicated. **c**, Extracting the single B cell RNA-seq data from a previous study[17] using pretreatment samples ($n = 16$). The fraction of *CD69*$^+$ B cells was higher in responders to ICB than in nonresponders ($n = 8$), but the fraction of *IGLL5*$^+$ B cells was not. The fraction of *IGLL5*$^-$ *CD69*$^+$ cells was also higher in responders. Plots of fraction of *IGHD*$^+$ and *IGHG*$^+$ B cells in relation to response to ICB therapy. *P* values from two-sided Wilcoxon test. In **a**, the centre lines in the box plot represent the median, the box limits represent the lower and upper quartiles, and the whiskers extend to the most extreme values within 1.5× IQR. **d**, Pearson correlation between expression of *CD69* and germinal centre genes (*CD83* and *CXCR4*) in data from a previous study[18]. Pie charts display the fact that the fraction of *CD83*$^+$ and *CXCR4*$^+$ B cells is increased among *CD69*$^+$ B cells. Expression >1 was used as a cut-off for being present. Seven hundred and fifty-three B cells without a present plasma-cell signature were analysed. *P* value from two-sided Fisher's exact test. **e**, **f**, Heat map of gene-expression values corresponding to our TLS signature (**e**) and TLS-hallmark genes from the literature (**f**). Blue corresponds to increased expression. Mal., malignant cells. In **e**, **f**, single cells from the seven cell types on the left are from ref. [18], and from the four cell types on the right are from ref. [17].

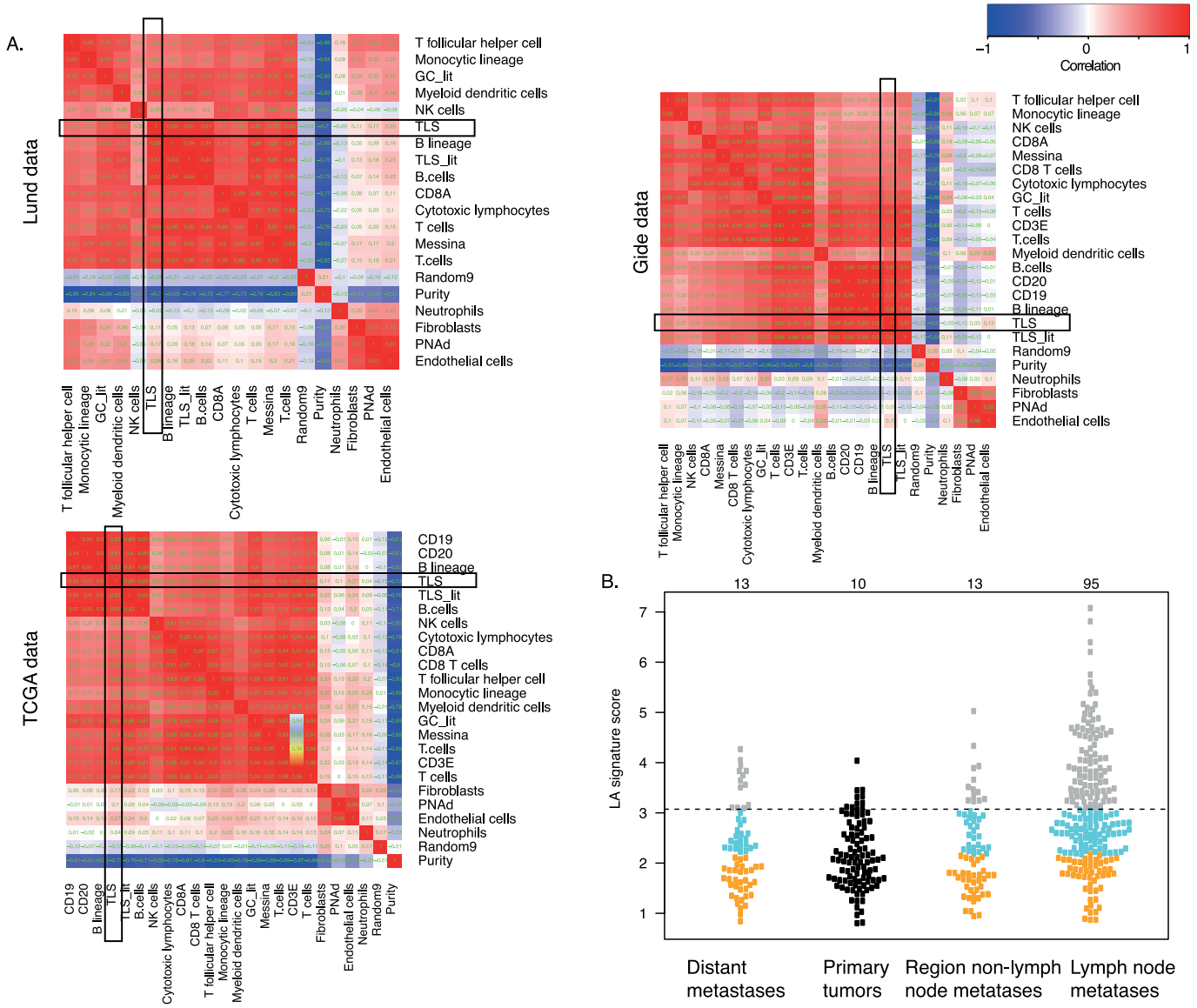

Extended Data Fig. 4 | Comparison of the derived TLS gene signature to other immune signatures. a, Pearson correlation plots of the data from the cohort obtained at Skåne University Hospital, Lund (top, $n = 160$), data from cases of melanoma metastasis in the TCGA (bottom, $n = 363$) and baseline data from a previous publication[22] (right, $n = 69$). Black box indicates the TLS signature. All signatures are taken from refs. [11,19,26]. Red, positive correlation; blue, negative correlation. **b**, TLS gene-signature scores in primary tumours in comparison to distant and lymph node metastases. The number of tumours assigned to the TLS^{high} category is indicated above the plot.

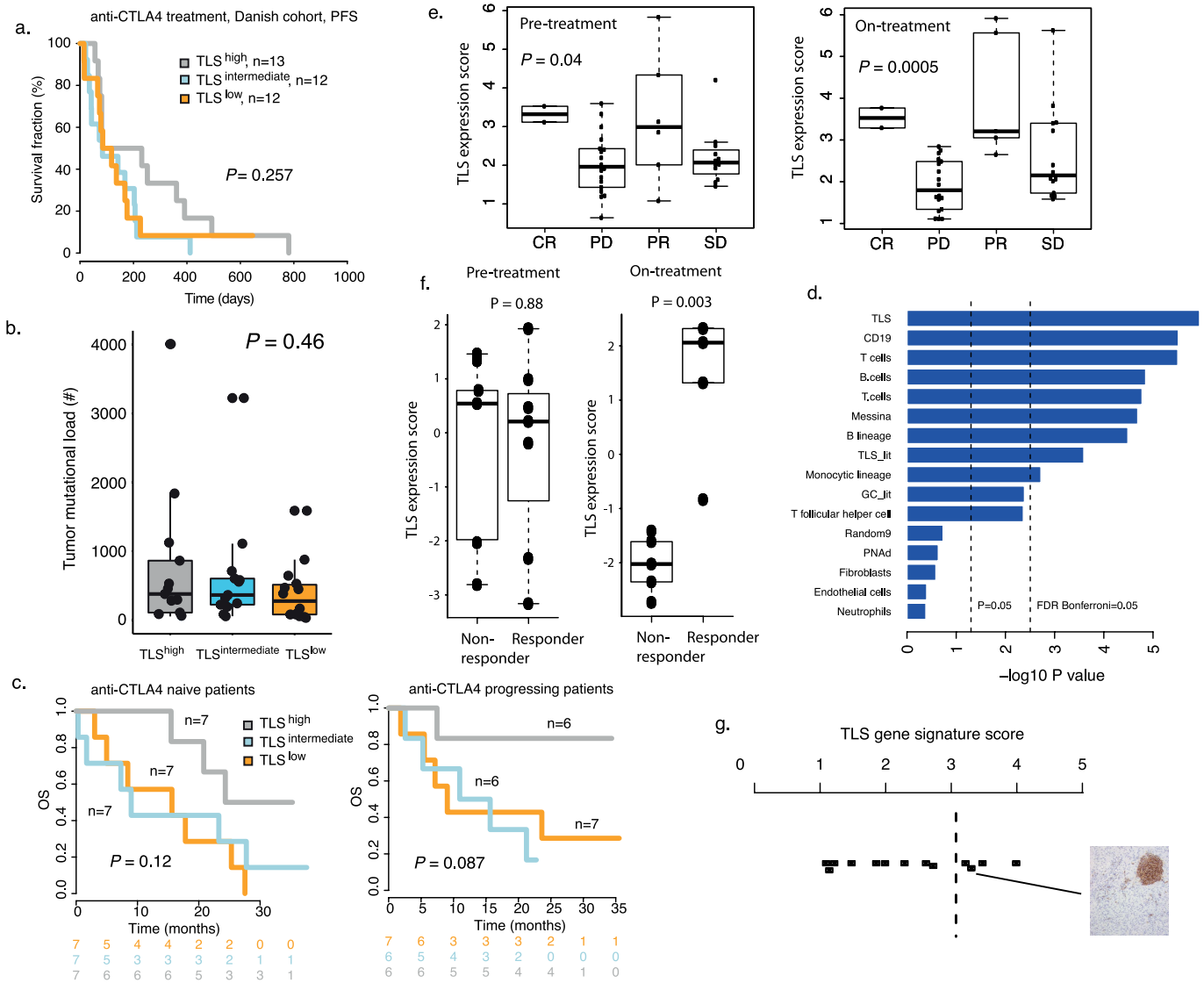

Extended Data Fig. 5 | TLS gene signature in cohorts treated by ICB. **a**, Progression-free survival (PFS) and TLS gene signature in the Danish cohort of patients treated with anti-CTLA4. *P* value from Cox regression. **b**, TLS gene signature in relation to tumour mutational load, in data from a previous publication[27] ($n = 40$ melanoma tumours). *P* value from Kruskal–Wallis test. **c**, Survival analyses on data from a previous study[28], stratified according to whether patients are naive to anti-CTLA4 treatment or have progressed on anti-CTLA4. *P* values from Cox regression. **d**, Meta Cox regression analysis across the four cohorts treated using ICB ($n = 186$). *P* values from Cox regression adjusted for study. **e**, TLS gene signature of pretreatment ($n = 16$) and on-treatment samples ($n = 10$) in relation to therapy response in data from a previous publication[30]. *P* value from two-sided *t*-test. **f**, TLS gene signature of pretreatment ($n = 38$) and on-treatment ($n = 39$) samples in relation to RECIST response in data from a previous study[28]. *P* value from ANOVA test. **g**, TLS gene-signature score in 13 melanoma tumours that were also stained for CD20 protein. As an example, the tumour with the third highest score had TLSs. The two top tumours also had TLSs, whereas the other tumours did not. In the box plots in **b**, **d**, **e**, centre lines represent the median, the box limits represent the lower and upper quartiles, and the whiskers extend to the most extreme values within 1.5× IQR.

Extended Data Table 1 | Clinical features of the 177-patient cohort, shown in correlation with CD8/CD20 immunological grouping

	ENTIRE COHORT (N=177)*	$CD8^+/CD20^+$ (N=44)	$CD8^+/CD20^-$ (N=57)	$CD8^-/CD20^-$ (N=74)	*P* VALUE
PATIENT CHARACTERISTICS					
GENDER N (%)					0.08
MALE	101 (57)	30 (70)	27 (47)	43 (60)	
FEMALE	72 (41)	13 (30)	30 (53)	29 (40)	
NA	4 (2)				
AGE AT DIAGNOSIS MEDIAN (RANGE)	65 (22-91)	66 (22-85)	64.5 (30-88)	65 (25-91)	
TUMOR CHARACTERISTICS					
STAGE					**0.003**
II	19	-	8	11	
III	104	35	29	39	
IV	50	7	20	23	
NA	4	2	-	1	
METASTASIS TYPE					**0.003**
LYMPH NODE	113	38	33	41	
SUBCUTANEOUS	35	3	12	20	
VISCERAL	10	1	5	4	
PRIMARY TUMOR	15	-	7	8	
NA	4	2	-	1	
CD8 IHC					
INFILTRATIVE N (%)	58 (33)	28 (64)	30 (53)	-	
CLUSTERED N (%)	43 (24)	16 (36)	27 (47)	-	
ABSENT N (%)	74 (42)		-	74 (100)	
NA N (%)	2 (1)				
CD3 IHC					
INFILTRATIVE N (%)	59 (33)	27 (61)	30 (53)	2 (3)	
CLUSTERED N (%)	52 (29)	17 (39)	27 (47)	8 (11)	
ABSENT N (%)	64 (36)	-	-	64 (86)	
NA N (%)	2 (1)				
CD20 IHC					
PRESENT N (%)	44 (25)	44 (100)	0 (0)	0 (0)	
ABSENT N (%)	131(74)	0 (0)	57 (44)	74 (56)	
NA N (%)	2 (1)				
PRIMARY TUMOR CHARACTERISTIC					
HISTOLOGICAL SUBTYPE					0.34
UNKNOWN PRIMARY N (%)	26 (15)	7 (16)	7 (12)	12 (16)	
SSM	36 (20)	10 (23)	13 (23)	13 (18)	
NM	57 (33)	15 (34)	21 (37)	21 (28)	
OTHER	17 (10)	2 (4)	3 (5)	12 (16)	
NA	39 (22)	10 (23)	13 (23)	16 (22)	

P values from Fisher's exact test, not adjusted for multiple testing.
*CD8 and CD20 status was missing for two patients.

Extended Data Table 2 | Univariate and multivariate Cox regression model analysis of immunological groupings in melanoma

	Univariate analysis		Multivariate analysis*	
	HR (CI)	*P*-value	HR (CI)	*P*-value
CD8				
infiltrative	1	-		
clustered	1.21 (0.65-2.26)	0.54		
absent	2.03 (1.20-3.43)	**0.009**		
CD20				
present	1	-		
absent	2.18 (1.24-3.82)	**0.007**		
CD8/CD20				
CD8+CD20+	1	-	1	-
CD8+CD20-	1.76 (0.93-3.35)	0.08	1.75 (0.91-3.37)	0.09
CD8-CD20-	2.54 (1.40-4.61)	**0.002**	2.60 (1.42-4.77)	**0.002**
*Stage**				
II	1	-	1	-
III	1.89 (0.58-6.07)	0.28	2.38 (0.73-7.73)	0.14
IV	7.84 (2.38-25.73)	**0.0007**	9.39 (2.84-31.04)	**0.0002**

Multivariate IHC marker and Stage

	CD8	*CD20*	CD8/CD20	*Stage*	*Metastasis type*	*Age*	*Gender*
Model 1	0.009			$4x10^{-9}$			
Model2		0.004		$1x10^{-8}$			
Model3			0.005	$9x10^{-9}$			
Model4			0.006		0.02		
Model5			0.005		0.03	0.70	0.58
Model6*			**0.006**	$8x10^{-7}$	0.68	0.69	0.76

TCGA multivariate cox analysis

	TLS signature	*Source site***	Age	*Gender*
Metastases only	**0.03**	0.02	0.01	0.56
All tumors including primary tumors	**0.01**	0.05	0.02	0.53

Hazard Ratios in TCGA And ICB Cohorts

	HR (95% CI)	**p-value**
TCGA Metastases		
TLS^{high}	1	-
$TLS^{intermediate}$	1.68 (1.10-2.56)	0.02
TLS^{low}	1.81 (1.20-2.74)	0.005
Danish Data		
TLS^{high}	1	-
$TLS^{intermediate}$	3.76 (1.23-11.45)	0.02
TLS^{low}	2.36 (0.76-7.29)	0.14
Van Allen Data		
TLS^{high}	1	-
$TLS^{intermediate}$	3.19 (1.09-9.35)	0.03
TLS^{low}	3.50 (1.17-10.51)	0.03
Gide Data		
TLS^{high}	1	-
$TLS^{intermediate}$	1.08 (0.33-3.53)	0.9
TLS^{low}	4.01 (1.47-10.99)	0.007
Riaz Data		
TLS^{high}	1	-
$TLS^{intermediate}$	2.95 (0.92-9.43)	0.07
TLS^{low}	4.72 (1.53-14.56)	0.007

Hazard ratios and confidence intervals in the bottom panel correspond to the Kaplan–Meier plots in Fig. 3.
*Model 6 includes CD8/CD20 groups, stage, type of metastasis, age and gender as covariates.
**Source site corresponds to primary tumour, regional lymph node, regional other and distant metastasis.

Extended Data Table 3 | Immune-related proteins investigated in the GeoMx analysis

Protein
4.1BB, CD137
ARG1
B7.H3
Bcl.2
Beta.2.microglobulin
CD11c
CD127
CD14
CD163
CD20
CD25
CD27
CD3
CD34
CD4
CD40
CD40L
CD44
CD45
CD45RO
CD56
CD66b
CD68
CD8
CD80
CD86
CTLA4
EpCAM
ER.alpha
FAPalpha
Fibronectin
FOXP3
GAPDH
GITR
GZMB
Her2.ErbB2
Histone.H3
HLA.DR
ICOS
IDO1
Ki.67
LAG3
MART1
Ms.IgG1
Ms.IgG2a
NY.ESO.1
OX40L
PanCk
PD.1
PD.L1
PD.L2
PR
PTEN
Rb.IgG
S100B
S6
SMA
STING
TGFB1
Tim.3
VISTA

Extended Data Table 4 | SAM analysis results to obtain the nine-gene TLS signature

Genes discriminating tumors with CD8 T cells alone compared to immune poor melanomas								*Genes discriminating tumors with TLS and CD8 T cells compared to melanomas with CD8 T cells alone*	
Gene	**Fold change**	**Gene**	**Fold change**	**Gene**	**Fold change**	**Gene**	**Fold change**	**Gene**	**Fold change**
C4orf7	5.850525	HLA-DMB	2.1769047	MFNG	1.7937715	HLA-C	1.6125638	DNASE1L3	2.7302825
CD8A	4.3367634	ARHGAP9	2.1595395	MS4A7	1.7918254	CTSC	1.6079848	CCL21	2.4948518
CXCL9	4.282619	LAMP3	2.1572433	TYROBP	1.7895821	RBM47	1.6064883	PLAC8	2.2948039
CD3D	4.109594	CD3G	2.1555102	ARHGAP25	1.7882159	CFB	1.605289	CD79A	2.1628115
NAPSA	3.9003344	EVI2B	2.151902	LAPTM5	1.7830758	EVI2A	1.6043215	CD79B*	2.1487825
CXCL13	3.878391	IL18BP	2.1482697	LOC387841	1.7806474	RNASE6	1.6032722	MGC29506	2.1386049
INDO	3.7693827	FCER1G	2.1476345	EBI3	1.779771	FPR3	1.5993513	CD48	2.1153479
CCL5	3.7572536	CAMK1G	2.1367993	P2RY8	1.7786007	ABI3	1.5974672	CD52	2.1007886
LTB	3.6854622	TBC1D10C	2.131732	C2	1.77573	RGS18	1.5973897	EIF1AY*	1.953128
CCL21	3.6670513	AIM2	2.129987	NCF1	1.774397	LY86	1.5972974	LTB	1.9445939
CCL19	3.634043	CD53	2.111374	PTPN22	1.7705708	PARP9	1.5966645	LRMP	1.9264982
IDO1	3.5465145	LCP1	2.1084743	FUCA1	1.7698385	OASL	1.5946562	FCRL3	1.9218179
GZMK	3.4980235	HLA-F	2.1038625	GIMAP6	1.76921	SERPINA1	1.590805	IGJ	1.907474
CXCL10	3.3749766	FGD3	2.0983796	BTK	1.7660133	SLCO2B1	1.5882876	CCL19	1.9025567
GZMA	3.32443	HLA-DRB4	2.096038	OAS2	1.7645061	SUSD3	1.5878158	BIRC3	1.8866026
LOC652775	3.3141112	BIRC3	2.0951495	OLR1	1.7627058	UBE2L6	1.586905	PTPRCAP	1.8761556
UBD	3.2973506	PYHIN1	2.0907834	GBP2	1.7621691	PSME2	1.5857576	NAPSB	1.8707682
CD69	3.232438	PRF1	2.0893168	TLR8	1.7585747	PLCL2	1.5817555	CD37	1.8535264
NKG7	3.2006474	FAM113B	2.0810633	EBI2	1.7581428	SAMD9L	1.5809402	CCR7	1.8436617
CD247	3.1996102	HCLS1	2.078721	RNF126P1	1.7579799	P2RY10	1.5796638	EAF2	1.8174217
CD2	3.148034	GVIN1	2.074809	IFIH1	1.7515248	PIK3CG	1.5796467	FAM46C	1.8072395
GBP5	3.1334765	TNFSF10	2.069712	CCR2	1.7498112	MX1	1.5793523	CD27	1.7974521
GZMB	3.0648828	HLA-DMA	2.0650768	AMICA1	1.7432792	ISG15	1.5779757	IRF8	1.792097
CCR7	3.0349138	RASGRP1	2.0589375	AIF1	1.7415568	CDC42SE2	1.5738891	SELL	1.7876798
CD79A	2.9795752	C1QC	2.056882	GLRX	1.7394656	P2RY13	1.5730076	PIM2	1.7812064
CD48	2.9609842	HLA-DPB1	2.0534782	FAM46C	1.7381114	PARVG	1.5702442	CORO1A	1.7604752
LOC647506	2.8764262	HLA-DOA	2.0447738	MARCO	1.7333692	VAMP5	1.5684881	HLA-DOB	1.7463384
HCP5	2.8615928	PSCDBP	2.0414143	CD86	1.7330478	FOLR2	1.5683817	CD3D	1.7436912
SPOCK2	2.8324168	C7	2.0402412	STX11	1.7318233	HLA-DQB2	1.5620639	PTGDS*	1.7368562
PTPRCAP	2.8146172	APOL3	2.0391428	APBB1IP	1.7280052	CD300LF	1.5616324	CLECL1	1.735072
LOC649143	2.8042858	PTPN6	2.038657	LYN	1.7253813	VCAM1	1.5614156	LOC606724	1.7307659
IL32	2.7964118	WAS	2.0366387	TNFAIP8	1.7246032	TNFAIP3	1.5603107	RBP5*	1.7290683
LAG3	2.7963312	BCL11B	2.0366046	INPP5D	1.724358	SLAMF7	1.5601757	UCP2	1.706331
HLA-DQA1	2.7800684	C20orf100	2.0273168	CYSLTR1	1.7242785	HCK	1.5587567	TBC1D10C	1.7048037
SLAMF6	2.7586188	CD37	2.0114977	MCOLN2	1.7232472	CARD11	1.558226	LIME1	1.682545
CD7	2.7440262	PRKCB	2.011462	SOD2	1.718578	CCL3	1.5579741	CD72	1.6630936
LOC100133678	2.7211967	LOC400759	2.0097654	AKNA	1.7166778	PIK3IP1	1.5557806	CCR6*	1.6473467
HLA-DRB6	2.713655	HLA-H	2.009027	TNFRSF1B	1.7134982	TSTD1	1.555676	TRAF3IP3	1.6443537
CD27	2.7128735	FGD2	2.0087543	IGSF6	1.7131412	DDX60	1.553378	LGALS2	1.642509
RARRES3	2.7052057	SLC40A1	2.0084155	CFD	1.7116679	IFIT2	1.553336	SKAP1*	1.6344548
GBP4	2.6934311	HLA-DRB3	2.0073037	PLCG2	1.7082311	CD72	1.5531305	VNN2	1.6247652
LOC651751	2.6899047	NCF1C	2.006084	ALOX5	1.7012193	SP140	1.5522988	PLCG2	1.6141123
LOC652694	2.685632	CECR1	2.0038574	DHRS9	1.7011156	ZFP36	1.5516263	SLAMF6	1.6129341
JSRP1	2.6221983	RASAL3	1.9993367	PPP1R16B	1.7008039	UBA7	1.5514268	PTPN6	1.605178
GIMAP7	2.6219752	GIMAP5	1.9982749	LAX1	1.6922069	BATF	1.5485026	CD247	1.6045387
IRF8	2.6158779	PIK3AP1	1.9907101	LST1	1.6902115	IFI27	1.547818	GAPT	1.6027378
PRKCB1	2.5978892	ITK	1.9889216	ACSL5	1.68995	CSF2RA	1.5462152	LAT*	1.5986894
LOC728835	2.573962	CD38	1.9883611	FCGR1B	1.6899358	NCF2	1.5452782	CD38	1.5831853
IGLL3	2.560279	CD96	1.9737343	HLA-E	1.6876732	TAP2	1.5432647	CETP*	1.5777292
LOC100133583	2.553927	PTPRC	1.9713553	PIM2	1.681412	DAPP1	1.5431949	PSCDBP	1.5753787
CD52	2.5466175	CCL18	1.9712074	ARHGAP30	1.680812	IFI35	1.5372068	ARHGAP9	1.5631298
NAPSB	2.5303907	GIMAP2	1.9646053	HLA-G	1.6804048	ALOX5AP	1.5365016	CD1D*	1.5562539
SH2D1A	2.5151858	CYBB	1.9622309	SLC7A7	1.6793996	ABCG1	1.5314059	LAX1	1.5507433
LOC649923	2.5026162	CXCL11	1.9613086	PSCD4	1.6785691	LYL1	1.5313303	C7	1.5440828
LOC652493	2.490692	PTGER4	1.9604341	CLEC4A	1.6785455	XAF1	1.5307403	CD6	1.5386331
LOC647450	2.4846182	ITGAL	1.9591348	KYNU	1.678476	RGS10	1.5273899	CD3G	1.5267668
CORO1A	2.4811893	MS4A6A	1.9552932	CTSH	1.6757919	FLI1	1.526178	DOCK8	1.5072867
LOC606724	2.4712005	TAP1	1.9535233	IL10RA	1.6756753	IRF7	1.5240406	PVRIG	1.5064694
HLA-DQB1	2.4548614	GIMAP1	1.943057	HAVCR2	1.6754664	IL4I1	1.5239596		
DNASE1L3	2.4548588	MGC29506	1.9380807	SEPP1	1.6752254	ADRB2	1.5232662		
GZMH	2.4348328	IGLL1	1.9257094	IL15	1.6723912	LAP3	1.5217831		
GBP1	2.4314487	DOCK2	1.9256791	PSTPIP2	1.6706566	APOBEC3G	1.5210005		
HCST	2.4196472	PLA2G7	1.9201738	UCP2	1.667601	TOX2	1.5196278		
PLEK	2.417525	CCL3L3	1.9036595	SIGLEC10	1.666853	LPXN	1.5194254		
FGL2	2.4134262	TRIM22	1.9034454	ZBP1	1.6624216	FBXO6	1.5154316		
CCL13	2.4028354	KLRD1	1.9017122	ITGB2	1.6614282	ASCL2	1.5137706		
IGJ	2.4006696	IFI44L	1.8944559	OAS1	1.6578766	AADACL1	1.5122902		
IRF1	2.3972383	C1QA	1.8862053	LOC647108	1.6575867	MYO1G	1.5105464		
LOC730415	2.377494	IKZF1	1.8854065	IFITM1	1.6569607	IFI6	1.5104185		
CCL4L2	2.3680255	ALDH2	1.8754903	CLECL1	1.65586	EAF2	1.5100641		
GNLY	2.3650563	DOCK8	1.8699276	ICOS	1.653902	LILRB3	1.5093257		
IFNG	2.3623235	SEMA4D	1.8665683	RASSF5	1.6529869	CSF1R	1.5070226		
IL2RB	2.347795	NCKAP1L	1.859875	C1S	1.651071	CYTH4	1.5061525		
EPSTI1	2.335121	ANKRD22	1.8569533	MS4A4A	1.6509206	MGAT4A	1.505879		
CCL4L1	2.3269346	SLA	1.8484899	LAIR2	1.6478871	LAT2	1.5024157		
LYZ	2.3133543	CTSS	1.8483866	LILRB5	1.644692	SLC31A2	1.5022907		
LOC731682	2.3117633	WARS	1.8480946	LILRB2	1.6428468	ATP8B4	1.5022835		
HLA-DPA1	2.3102183	SASH3	1.8472831	PSMB8	1.642432	RCSD1	1.5018578		
LOC642073	2.3056629	RGS1	1.8432442	CXCR3	1.6415471	GCH1	1.5016657		
HLA-B	2.303435	C1orf162	1.8429196	SPI1	1.6396817	LILRA5	1.5010871		
ADAMDEC1	2.2967832	CRKRS	1.8394536	CXCR4	1.6376555				
STAT1	2.2745712	LRMP	1.8371218	FCGR1A	1.6370385				
CD74	2.273994	SRGN	1.8356284	DEF6	1.6362371				
C1QB	2.2717638	CEBPA	1.8305081	ITGB7	1.6362158				
PVRIG	2.2529182	VNN2	1.8215137	NCF4	1.6340253				
CCL8	2.252525	GIMAP8	1.8203901	AGPAT9	1.6268378				
LOC642113	2.251248	CASP1	1.8195084	LGALS2	1.6255531				
FAM26F	2.2444625	DENND2D	1.8194357	CD163	1.6254405				
LIME1	2.2311883	GMFG	1.8193122	FGR	1.62524				
SELL	2.2240884	GPR65	1.8181477	ADD3	1.6250473				
PSMB9	2.2207227	MAP4K1	1.8174882	ANKRD29	1.6237315				
RAC2	2.2163737	ISG20	1.8124862	FCN1	1.623711				
IL7R	2.215939	FBP1	1.8124799	MIR155HG	1.6234839				
FYB	2.2151234	CLEC12A	1.8113737	CD209	1.6229211				
LOC401845	2.2078538	CXCL12	1.8111467	LILRB4	1.6225767				
HLA-DRA	2.1994276	HLA-DOB	1.807083	IFIT3	1.6202953				
KLRB1	2.1980007	STAT4	1.8062018	KIR2DL4	1.6192334				
PLAC8	2.1869752	SLAMF8	1.8041736	TRAF3IP3	1.6186843				
GIMAP4	2.1838875	IFI30	1.7981355	GAPT	1.6185887				
FCRL3	2.1787016	RSAD2	1.7952874	TLR7	1.6158199				
FAIM3	2.1784108	PRKCH	1.7944446	STK17B	1.6147563				
CD6	2.1783032	SAMSN1	1.7943485	SLC15A3	1.6138071				

*Gene unique to the tumours with TLS.

Extended Data Table 5 | Clinical features of the cohorts treated by ICB

	ENTIRE COHORT (N=201)	TLS^{HIGH} (N=44)	TLS^{INT} (N=57)	TLS^{LOW} (N=74)
DANISH ANTI-CTLA4 TREATED COHORT				
COHORT N (%)	37 (18)	13 (35)	12 (32)	12 (32)
AGE AT TREATMENT MEDIAN (RANGE)	63 (33-84)	65 (34-77)	64 (34-80)	59 (33-80)
LDH LEVELS MEDIAN (RANGE)	207 (125-545)	211 (136-302)	184 (147-434)	205 (143-545)
METASTATIC SITE				
SKIN	11	1	5	5
LYMPH NODE	14	6	5	3
CNS	3	1	0	2
LUNG	3	1	1	1
OTHER	3	1	1	1
NA	3	-	-	-
VAN ALLEN ANTI-CTLA4-TREATED COHORT (N=40)[1]				
AGE AT DIAGNOSIS (RANGE)	59 (32-83)	57 (33-83)	61 (43-77)	59 (32-71)
GENDER (%)				
MALE	26 (65)	10 (38)	7 (27)	9 (35)
FEMALE	14 (35)	3 (21)	6 (43)	5 (36)
RIAZ ANTI-PD1 TREATED COHORT (N=40)[2]				
PRIOR ANTI-CTLA4 TREATMENT (%)				
YES	19 (48)	8 (42)	7 (37)	4 (21)
NO	21 (52)	5 (24)	6 (29)	10 (48)
M STAGE				
M1A	10	4	4	2
M1B	7	4	1	2
M1C	16	4	5	7
NA	6	-	3	3
GIDE ANTI-PD1 TREATED COHORT (N=61)[2]				
GENDER N (%)				
MALE	45 (65)	14 (31)	16 (36)	15 (33)
FEMALE	24 (35)	9 (38)	7 (29)	8 (33)
AGE MEDIAN (RANGE)	61 (24-90)	68 (24-78)	62 (40-82)	58 (42-90)
METASTATIC SITE				
LYMPH NODE	19	9	6	4
SUBCUTANEOUS	43	10	17	16
LUNG	3	3	-	-
OTHER	4	1	-	3

nature research

Corresponding author(s): Göran Jönsson

Last updated by author(s): Nov 7, 2019

Reporting Summary

Nature Research wishes to improve the reproducibility of the work that we publish. This form provides structure for consistency and transparency in reporting. For further information on Nature Research policies, see Authors & Referees and the Editorial Policy Checklist.

Statistics

For all statistical analyses, confirm that the following items are present in the figure legend, table legend, main text, or Methods section.

n/a	Confirmed	
☐	☒	The exact sample size (*n*) for each experimental group/condition, given as a discrete number and unit of measurement
☐	☒	A statement on whether measurements were taken from distinct samples or whether the same sample was measured repeatedly
☐	☒	The statistical test(s) used AND whether they are one- or two-sided *Only common tests should be described solely by name; describe more complex techniques in the Methods section.*
☐	☒	A description of all covariates tested
☐	☒	A description of any assumptions or corrections, such as tests of normality and adjustment for multiple comparisons
☐	☒	A full description of the statistical parameters including central tendency (e.g. means) or other basic estimates (e.g. regression coefficient) AND variation (e.g. standard deviation) or associated estimates of uncertainty (e.g. confidence intervals)
☐	☒	For null hypothesis testing, the test statistic (e.g. *F*, *t*, *r*) with confidence intervals, effect sizes, degrees of freedom and *P* value noted *Give P values as exact values whenever suitable.*
☒	☐	For Bayesian analysis, information on the choice of priors and Markov chain Monte Carlo settings
☐	☒	For hierarchical and complex designs, identification of the appropriate level for tests and full reporting of outcomes
☒	☐	Estimates of effect sizes (e.g. Cohen's *d*, Pearson's *r*), indicating how they were calculated

Our web collection on statistics for biologists contains articles on many of the points above.

Software and code

Policy information about availability of computer code

Data collection	The following software was used in the study: R version 3.5.1 with base/standard packages and additional packages: estimate_1.0.13, GLAD_2.46.0, limma_3.38.3, survival_2.42-3, swamp_1.4.1 and TxDb.Hsapiens.UCSC.hg19.knownGene_3.2.2 . SAM analysis in the TMeV tool (v 4.8.1). HISAT (v. 2.1.0), Stringtie (v. 1.3.3b) (https://ccb.jhu.edu/software/stringtie/). samtools 1.9 (https://sourceforge.net/projects/samtools/files/samtools/). CONTRA 2.0.3. (http://contra-cnv.sourceforge.net/)
Data analysis	The following software was used in the study: R version 3.5.1 with base/standard packages and additional packages: estimate_1.0.13, GLAD_2.46.0, limma_3.38.3, survival_2.42-3, swamp_1.4.1 and TxDb.Hsapiens.UCSC.hg19.knownGene_3.2.2 . SAM analysis in the TMeV tool (v 4.8.1). HISAT (v. 2.1.0), Stringtie (v. 1.3.3b)) (https://ccb.jhu.edu/software/stringtie/). samtools 1.9 (https://sourceforge.net/projects/samtools/files/samtools/). CONTRA 2.0.3. (http://contra-cnv.sourceforge.net/)

For manuscripts utilizing custom algorithms or software that are central to the research but not yet described in published literature, software must be made available to editors/reviewers. We strongly encourage code deposition in a community repository (e.g. GitHub). See the Nature Research guidelines for submitting code & software for further information.

Data

Policy information about availability of data

All manuscripts must include a data availability statement. This statement should provide the following information, where applicable:

- Accession codes, unique identifiers, or web links for publicly available datasets
- A list of figures that have associated raw data
- A description of any restrictions on data availability

All relevant data are available and are included with the manuscript as source data. Digital spatial profiling data used in Fig. 2 and gene expression microarray data from anti-CTLA4 treated patients are available as source data. Data from public repositories were accessed from GSE65904 (Cirenajwis et al.), TCGA data portal SKCM level 3 release 3.1.14.0 (TCGA data), PRJEB23709 (Gide et al.), https://github.com/riazn/bms038_analysis/tree/master/data (Riaz et al.), GSE115978 (Jerby-Arnon et al.) and GSE120575 (Sade-Feldman et al.). Any other relevant data and code can be obtained from the corresponding authors upon reasonable request.

Field-specific reporting

Please select the one below that is the best fit for your research. If you are not sure, read the appropriate sections before making your selection.

☒ Life sciences ☐ Behavioural & social sciences ☐ Ecological, evolutionary & environmental sciences

For a reference copy of the document with all sections, see nature.com/documents/nr-reporting-summary-flat.pdf

Life sciences study design

All studies must disclose on these points even when the disclosure is negative.

Sample size	These cohorts are unique and sample sizes are for the Lund cohort (n=177) and the Danish anti-CTLA4 (n=37). These are cohorts collected during a long time and we believe these are sufficient to askt the questions we put forward in the manuscript. In addition, we use cohorts where data are available in public repositories.
Data exclusions	Patients were only excluded from analyses if the tissue specimen did not include any tumor cells as determined by a dermatopathologist
Replication	The derived TLS gene expression signature was firmly validated in several different datasets across multiple gene expression platforms.
Randomization	Randomization is not relevant for this study as we are analysing tumor specific phenotypes.
Blinding	Immunostaining evaluation were done blinded by three independent readers of which one was a board-certified dermatopathologist.

Reporting for specific materials, systems and methods

We require information from authors about some types of materials, experimental systems and methods used in many studies. Here, indicate whether each material, system or method listed is relevant to your study. If you are not sure if a list item applies to your research, read the appropriate section before selecting a response.

Materials & experimental systems

n/a	Involved in the study
☐	☒ Antibodies
☒	☐ Eukaryotic cell lines
☒	☐ Palaeontology
☒	☐ Animals and other organisms
☐	☒ Human research participants
☒	☐ Clinical data

Methods

n/a	Involved in the study
☒	☐ ChIP-seq
☒	☐ Flow cytometry
☒	☐ MRI-based neuroimaging

Antibodies

Antibodies used	The following antibodies are used in this study. CD3 (polyconal, cat no A0452, lot no 20066809, Dako/Agilent), CD8 (clone C8/144B, cat no M7103, lot no 20029542, Dako/agilent), CD20 (clone L26, cat no. 760-2531, lot no 00064779, Dako/Agilent), SOX10 (clone BC34, cat no. ACI 3099 A, C, Biocare), B2M (polyclonal, cat no. A0072, lot no 00066626, Agilent/Dako), Ki67 (clone MIB-1, cat no. GA626, lot no 20027876, Dako/agilent) . For immunofluoroscence rabbit-anti-CXCR5 (cat no. 3180237-9, lot no GR3229212-1, abcam) and rabbit-anti-CXCL13 (cat no NBP2-1604155, lot no 0141712Da843058, Novus Biologicals)
Validation	Antibodies used in this study are well validated. This is clearly demonstrated by the manufacturer as well as the vast number of citations refereing to the antibodies. In addition, the SOX10 and CD20 stainings were performed at a Swedish clinically approved diagnostic laboratory. The following information is available for each antibody. CD3 (polyconal, cat no A0452) - Rabbit Anti-Human for IHC - In Western blotting, the antibody detects bands of the expected

molecular weights for CD3 antigens. The antibody recognizes CD3e in both a T-cell line (Jurkat) and a natural killer cell line (NK11), but does not react with lysates prepared from several B-cell lines (Raji, Ramos and JY), a myeloid cell line (U937) or a colon carcinoma cell line (Colo-205).
In immunoprecipitation from Nonidet P40 lysates of surface-iodated T lymphoblasts, the antibody precipitates the g (26 kDa), d (21 kDa) and e (19 kDa) chain of the CD3 molecule, similar to the precipitation pattern seen using the well-characterized monoclonal mouse anti-human CD3, clone UCHT1.
In ELISA, the antibody labels the CD3 peptide used as immunogen.
CD8 (clone C8/144B, cat no M7103) - Mouse Anti-Human - SDS-PAGE analysis of immunoprecipitates formed between lysates of 125I-labeled human T lymphoblasts and the antibody shows reaction primarily with a 32 kDa polypeptide corresponding to CD8α.
CD20 (clone L26, cat no. 760-2531) - Mouse Anti-Human - The antibody was clustered as anti-CD20 at the Fifth International Workshop and Conference on Human Leucocyte Differentiation Antigens held in Boston 1993. SDS-PAGE analysis of immunoprecipitates formed between 125I-labeled tonsil cell lysate and the antibody shows reaction primarily with 30 kDa and 33 kDa polypeptides. Studies using COS-1 cells transfected with cDNA encoding the CD20 molecule, indicate that the antibody labels an intracytoplasmic epitope localized on the CD20 molecule.
SOX10 (clone BC34, cat no. ACI 3099 A, C, Biocare) - Mouse Anti-Human - Nuclear staining of SOX10 [BC34] was observed in 96.4% (106/110) of cases of cutaneous melanoma and 83.9% (73/87) of cases of metastatic melanoma (Table 1). Staining of SOX10 [BC34] was also observed in spindle cell melanoma (100%, 19/19), desmoplastic melanoma (96.6%, 28/29), benign nevi (100%, 20/20) and schwannomas (100%, 28/28). SOX10 [BC34] nuclear staining was observed in the expected normal tissues: oligodendrocytes in cerebrum and cerebellum, myoepithelial cells in breast and salivary glands, melanocytes in skin, and Schwann cells in peripheral nerve.
B2M (polyclonal, cat no. A0072) - rabbit anti-human - Crossed immunoelectrophoresis: B2M precipitation curve is visible in th eusage of 12.5 ul A0072 per cm2 gelsurface against concentrated urine from patients with tubular proteinuria. Using 2 ul human plasma no precipitation is observed. Staining: Coomassie Brilliant Blue.
Ki67 (clone MIB-1) - Mouse Anti-Human - In Western blotting of lysates of the multiple myeloma cell line, IM-9, the MIB-1 antibody labels bands of 345 and 395 kDa, identical to the bands labeled by the original Ki-67 antibody. Furthermore, Western blotting and competitive binding experiments clearly demonstrate that MIB-1, like the original Ki-67 antibody, reacts with an epitope encoded by a 66 bp repetitive element in the Ki-67 gene. In immunohistochemistry, the MIB-1 and the Ki-67 antibodies provide identical staining patterns on serial tonsillar frozen sections. The MIB-1 antibody recognizes native Ki-67 antigen and recombinant fragments of the Ki-67 molecule.
IF-specific antibodies
rabbit-anti-CXCR5 (cat no. 3180237-9) -rabbit anti-human - In Western Blot one specific band is observed in mouse B cells. Additional evidence comes from IF experiments on lymphoma cells.
rabbit-anti-CXCL13 (cat no NBP2-1604155) - rabbit anti-human - In Western Blot one specific band is observed in 293T whole extract. Additional evidence comes from IF experiments on HepG2 cells.

Human research participants

Policy information about studies involving human research participants

Population characteristics	Overall, 104 patients had regional metastatic disease, 50 distant disease and 19 local disease. Four patients were of unknown stage. This is a historic cohort collected between 2000 and 2012. 57% were male patients, the age at diagnosis were on average 65. 64% were lymph node metastases, 20% were subcutaneous metastases, 6% were visceral metastases and 8% were primary tumors.
Recruitment	The Lund pre-checkpoint inhibitor cohort was collected prospectively from 1997-2012 at the Dept of Surgery, Skåne University Hospital in Sweden. Only patients where sufficient tissue was available were included in the study. The Danish anti-CTLA4 treated cohort is retrospective and includes all patients recieving first-line anti-CTLA4 treatment up until year 2016.
Ethics oversight	This study was approved by the Regional Ethics Committee at Lund University (Dnr. 191/2007 and 101/2013). The sample cohort, representing a population-based retrospective collection (n=177), was obtained at the Department of Surgery at Skåne University Hospital. We also collected paraffin embedded tumor tissue from 119 patients of which 37 patients received anti-CTLA4 as first-line therapy. These patients were collected in Denmark and available biopsy was obtained a maximum of six months before therapy start. This study was approved by the regional ethical committee (H-15010200).

Note that full information on the approval of the study protocol must also be provided in the manuscript.